Plasma Sources
Science and
Technology

PAPER • **OPEN ACCESS**

Determination of the accuracy of actinometry and line ratio techniques in an O_2 glow discharge: I. Comparison of absolute oxygen atom densities with CRDS measurements

To cite this article: E Baratte *et al* 2026 *Plasma Sources Sci. Technol.* **35** 015009

Plasma Sources Science and Technology

OPEN ACCESS

RECEIVED
30 June 2025

REVISED
8 October 2025

ACCEPTED FOR PUBLICATION
26 November 2025

PUBLISHED
16 January 2026

PAPER

Determination of the accuracy of actinometry and line ratio techniques in an O_2 glow discharge: I. Comparison of absolute oxygen atom densities with CRDS measurements

E Baratte[1], L Kuijpers[2,3,*], T Silva[4], V Guerra[4], M C M van de Sanden[2,3], J-P Booth[1] and O Guaitella[1,*]

[1] LPP, CNRS, École Polytechnique, Sorbonne Université, Université Paris-Saclay, IP-Paris 91128 Palaiseau, France
[2] Department of Applied Physics, Eindhoven Institute for Renewable Energy Systems, Eindhoven University of Technology, Eindhoven, The Netherlands
[3] Dutch Institute For Fundamental Energy Research, De Zaale 20, 5612 AJ Eindhoven, The Netherlands
[4] Instituto de Plasmas e Fusão Nuclear, Instituto Superior Técnico, Universidade de Lisboa 1049-001, Lisboa, Portugal
* Authors to whom any correspondence should be addressed.

E-mail: l.kuijpers@tue.nl and olivier.guaitella@lpp.polytechnique.fr

Keywords: actinometry, CRDS, atomic oxygen, O2 plasma, cross sections, glow discharge

Abstract

The accuracy of oxygen atom density measurements in plasmas by optical emission actinometry was tested by comparison to simultaneous direct absorption measurements on the $^1D_2 \leftarrow {}^3P_2$ transition by cavity ringdown spectroscopy (CRDS). The accuracy of the latter technique depends only on the accuracy to which the transition probability is known. Measurements were performed on a glow discharge in O_2 operating between 0.5 and 5 Torr, and using both Ar and Xe as the actinometer gas. The rate constants for electron impact excitation, and thus the actinometry calibration factors, were calculated from the (measured) reduced electric field using a Boltzmann equation solver (Loki-B). Several sets of cross-section were tested for the EEDF calculation and for the electron impact excitation to the specific levels of O, Ar and Xe used for actinometry. The best results were obtained with the IST Lisbon cross-section set for O_2 and O, and the BSR500 excitation cross-sections for Ar and Xe. Good agreement with the CRDS trends and absolute values was observed when using Xe as the actinometer gas, whereas with Ar the trends were well reproduced but it was necessary to increase the electron impact cross-section of the transition $Ar(^1S_0 \rightarrow 2p_1)$ of the BSR500 database by a factor of 3 ± 0.3 to reproduce the absolute values.

1. Introduction

Transient atomic species play a key role in reactive plasmas but are challenging to measure. Among the many techniques devised to measure the densities of atomic species, optical emission spectroscopy is the most widely employed due to its non-perturbative nature, its experimental simplicity, and its ability to monitor a wide range of transient species (*e.g* H, O, N, or F) with spatial and temporal resolution. In optical emission actinometry [1, 2] the absolute density of a given species (often atomic) is estimated from the ratio of the optical emission intensity from an excited state of that species to that from an actinometer gas (typically a noble gas) introduced in a low fraction (typically under 5%, in order to minimize plasma perturbation).

Actinometry is based on the assumption that the observed excited state is dominantly populated by electron impact on the ground state, so that the emission intensity is proportional to the ground state density. The ground state density can then be estimated by calculating the electron impact excitation rate coefficient (as well as accounting for collisional and radiative quenching of the excited state if this is significant). This calculation requires knowledge of the excitation cross-section as well as the electron energy distribution function (EEDF). The EEDF can be calculated in a DC glow discharge for a given value of the reduced electric field if the complete set of collision cross-sections of the bath gas is

known. The technique has also been applied a number of other discharge scenarios, using a number of simplifying hypotheses with different degrees of complexity. Ricard *et al* [3]. assumed simple proportionality between the intensities and the densities, in order to estimate the N density in N_2–O_2 and N_2–H_2 microwave discharges, using Ar as actinometer. The proportionality coefficient was determined using TALIF measurements. Unusually, the Ar line at 811.5 nm (further noted Ar811) was used for Ar intensity in [3]. A more rigorous approach uses calculation of the EEDF in the initial mixture. Pagnon *et al* [4], compared actinometry measurements of O atoms to VUV absorption measurements in O_2 glow discharges at a few Torr, with numerical computation of the EEDF from the Boltzmann equation. Collisional quenching of the radiating states (radiating the lines at 777 and 844 nm for O and at 750 nm for Ar) was also taken into account. Britun *et al* compared O actinometry in HiPIMS Ar–O_2 discharges between 3 and 20 m Torr to TALIF measurements, calculating the rate coefficients assuming a Maxwellian EEDF with a temperature of 2 eV. They also included the effect of metastables states of Ar (but neglected those of O) on the population of the levels radiating the 8 Ar lines used for actinometry. Czerwiec *et al* [5] computed the rate coefficients assuming a Maxwellian EEDF in a low pressure N_2 ICP. The calculation also included collisional quenching of the Ar $2p_1$ and $2p_9$ radiating respectively the lines at 750 and 811 nm (respectively further designed as Ar750 and Ar811) lines used. Morillo-Candas *et al* [6], measured O atoms in a CO_2 glow discharge between 1 and 5 Torr, obtaining the rate coefficients from a Boltzmann solver computing the EEDF of the CO_2-Ar mixture using the measured reduced electric field. They only used the Ar750 line for Ar, but studied both the lines at 777 and 845 nm for O (respectively further noted as O777 and O845), with collisional quenching for all 3 levels. In this case the effect of the dissociation products on the EEDF as taken into account. Tsutsumi *et al* [7], calculated the EEDF for different dissociation degrees of O_2 to estimate the O atom density in a low pressure O_2–Ar CCP. The collisional quenching of the O845, O777 and Ar750 lines was again included. In [8–10], which investigate H and OH densities and water traces in a He:Ar:Xe glow discharge containing traces of water vapor, the computation of the EEDF was iterated to allow for dissociation products. Several lines are observed for the species of interest: a molecular band of OH at 306 nm, the emission of H at 656.3 nm and two lines of O (O777 and O845). Both Xe and Ar emission lines were used as actinometers (at respectively 823.1 and 750.5 nm). As opposed to most cases where a 'general' collisional quenching rate is used to describe the collisional quenching of the radiating levels by all the species of the plasma, the quenching of each radiating level by each species was described by a collisional quenching coefficient. At low pressure the EEDF can be measured by Langmuir probe. Lopaev *et al* [11], estimated N, F and O atoms densities in low-pressure glow discharges using Kr as actinometer. They used two lines for Ar (Ar750 and Ar811) as well as two for O (O845 and O777) and included quenching of the radiating levels by collision with a generic partner M.

The estimation of absolute densities by actinometry requires knowledge of basic collision data, including excitation cross-sections and complete sets of collision cross-sections for EEDF computation. Evidently, the accuracy of the method depends directly on the quality of this basic data. Although some studied have compared actinometry to other diagnostics [4, 6], obtaining quantitative agreement of absolute densities remains challenging and is highly dependent on the choice of collisional data. Although many cross-sections are available in literature, there are often large discrepancies; choosing the optimal set can be problematic, leading to large uncertainty in the results. This study is divided into two parts. The first part explores the problems that arise in actinometric measurements of oxygen atom densities, and provides a reliable set of parameters to determine O atom densities from actinometry using either Ar or Xe. The actinometry measurements are compared to cavity ring down spectroscopy (CRDS) measurements of the ground-state O atom density, which is assumed to provide accurate absolute densities of O atoms. Measurements were made in a DC glow discharge in pure O_2, O_2:Ar and O2:Xe at pressures between 0.5 and 5 Torr. A line intensity simulation was used to test the cross-sections for each line. The results are then confirmed by direct comparison the results to simultaneous CRDS measurements. In the second part of this work [12], the optimised collision data chosen in this paper are used for actinometry, and a method is proposed for the determination of the reduced electric field from the intensity ratios of actinometer lines.

As already mentioned, previous studies [4, 6] have already proposed quantitative comparisons between densities obtained by actinometry and other diagnostic techniques. The originality of this work is to provide much stronger constraints on the choice of the collisional data used for the actinometry analysis by three means:

1. The analysis of the gas pressure and discharge current trends of the intensities of each individual emission line (not the line ratios) imposes much stronger constraints on the cross section set considered for oxygen atoms and for the actinometer

2. Not only does this work propose a comparison of actinometric results with another, more accurate, measurement method (namely CRDS), but this comparison is carried out with simultaneous measurements, in a particularly homogeneous discharge, with two different actinometers gases (Ar and Xe)
3. Analysis of the accuracy of the results obtained with the different effective cross-sections available in the literature is evaluated not only on the basis of the O atom densities compared with the CRDS results (the subject of part I of this work), but also with the reduced electric fields obtained by a line ratio technique using the same sets of effective excitation cross-sections for the 2 actinometer gases considered (the subject of part II of this article [12]).

This combined approach makes it possible to provide very strong constraints, in particular for the excitation cross sections for O, Ar and Xe. Indeed, if a unique set of excitation cross-sections can reproduce not only the individual line intensity variations, but also accurately indicates the O atom density (part I) and the reduced electric field (part II, [12]) from the line intensity ratios, then the excitation cross-sections can be considered to be accurate within the reduced electric field range explored in this work.

2. Experimental setup

A low-pressure glow discharge (between 0.5 and 5 Torr) was chosen for this study because it is reproducible, axially homogeneous in the positive column, the electric field (E) can easily be measured, and the electron density (n_e) can be varied simply by controlling the current. A schematic of the setup is shown in figure 1. The glow discharge is ignited in a 68 cm long cylindrical pyrex reactor of radius 1 cm. The electrodes are situated in side-tubes perpendicular to the axis of the tube, so that measurements take place only in the positive column. The gases are supplied to the tube by three mass flow controllers and the ensemble is pumped by an Edwards XDS pump. The tube is closed on both sides by two highly reflective mirrors (R>0.9997) which constitute the optical cavity of the CRDS system [13]. The mirror on one side is mounted on a piezoelectric actuator to enable longitudinal mode-matching. The discharge current is supplied by a stabilized DC power supply (FUG). Optical emission emitted perpendicular to the discharge axis is collected by a lens of focal length 5 cm positioned on the side of the tube, with its focal point at the center of the tube. The collimated beam is then focused onto the entrance slit of a spectrometer (Princeton Instruments Isoplane 320) by another lens of focal length 3.5 cm. The entrance slit of the spectrometer is set to 2 mm for all experiments. A grating of 1200 g mm^{-1} blazed at 500 nm is installed in the spectrometer. A photomultiplier tube Hamamatsu R13456 is mounted at the output of the spectrometer. For each tested conditions, the spectrometer sweeps over each line with a resolution of 0.02 nm and an integration time of 10 ms per point. The electric field is measured with two floating tungsten pins reaching inside the positive column of the glow discharge. The voltage difference between the pins is measured by a high-impedance voltage divider, giving the electric field. An almost identical setup was used in [14].

The conditions studied in this experimental study are given in table 1. The reduced electric field E/N varied between 90 Td at 0.5 Torr and 45 Td at 5 Torr.

3. CRDS

CRDS using a tunable single-mode diode laser is a reliable method to measure the absolute atomic density of oxygen as well the gas temperature (from the Doppler profile of the transition). The principles of this technique have been described in detail, *e.g* by Berden and Engeln [15]. CRDS was used for example by Booth *et al* [16] to measure fluorine-containing radicals in a low pressure RF plasma. This technique can be applied to numerous other species, for example Stancu *et al* [17] measured $N_2(A)$ in atmospheric pressure nanosecond discharges. The CRDS setup coupled to a low-pressure glow discharge used here has been presented previously [14].

Although the CRDS technique requires sophisticated equipment, the determination of the (line-integrated) atom density from the signal depends only on the simple Beer–Lambert law; measurements of relative density variations (as discharge conditions are changed) can be considered to be highly accurate, and the absolute accuracy of the measurement principally depends upon the accuracy to which the line-strength is known. reputedly ± 7% [18]. In this case the ground state of atomic oxygen is probed directly, unlike actinometry which probes electronically excited states. In this work the $O(^3P_2) \leftrightarrow O(^1D_2)$

Table 1. Experimental conditions used in this study.

Pressure	0.5–5 Torr
E/N	90–45 Td
Current	40 mA
Mixture	Pure O_2 / 95:5 O_2−Ar / 98:2 O_2−Xe
total flow	7.4 sccm

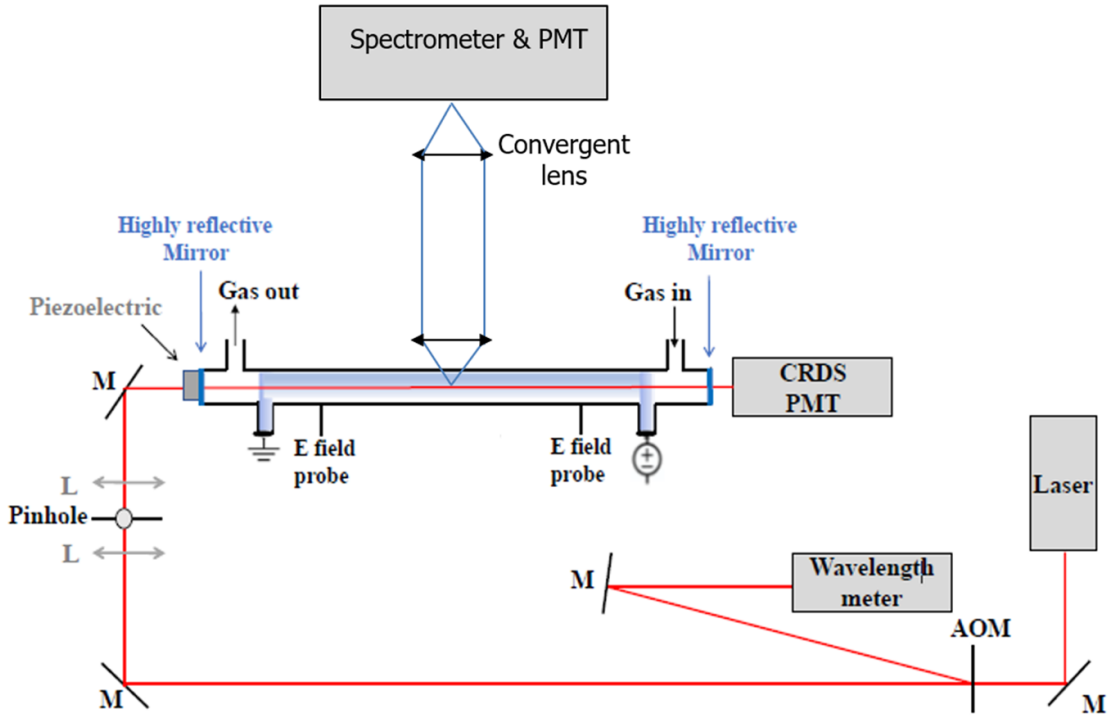

Figure 1. Experimental setup. The low-pressure DC glow discharge is ignited in a pyrex tube in a plug-flow configuration. The discharge is coupled with a Laser and a PMT for CRDS. The light emitted by the discharge perpendicular to the axis is sampled and sent to a spectrometer for actinometry.

transition at 630 nm is used, for which the integrated cross-section is given by [14]:

$$\sigma_{\text{int}} = \int \sigma_{\text{low}}^{\text{up}} d\nu = \frac{g_{\text{up}}}{g_{\text{low}}} \frac{A_{\text{low}}^{\text{up}} \lambda^2}{8\pi} = 2.9810^{-23} \text{cm}^3 \tag{1}$$

with $A_{\text{low}}^{\text{up}}$ the Einstein coefficient of the transition (taken from NIST), g_{up} is the degeneracy of the upper level $O(^1D_2)$, g_{low} the degeneracy of the lower level $O(^3P_2)$. The total density of the $O(^3P)$ state is deduced from the population of $O(^3P_2)$ by assuming thermal equilibrium across the other spin-orbit levels:

$$\left[O\left(^3P\right)\right] = \frac{\sum_j g_j e^{-E_j/kT} \left[O\left(^3P_2\right)\right]}{g_2}. \tag{2}$$

The CRDS setup is shown in figure 1. The tunable cw laser beam is provided by an external cavity diode laser (Toptica DLPro). The laser linewidth is of a few 10^{-7} cm^{-1} with a jitter below 10^{-3} cm^{-1}, tunable between 630.2087 and 630.1991 nm). Part of the laser beam is sampled with a beamsplitter and directed into a wavemeter (HighFinesse WS8) to monitor the laser wavelength. The main laser beam passes through an opto-acoustic modulator and coupled into the optical cavity through one spherical high-reflectivity mirror (R∼0.9999 at 630 nm). This mirror is mounted on a piezo-electric translator which moves with an amplitude of more than one λ at a frequency of 30 Hz. The beam exits the cavity through a second highly reflective mirror and is detected by a photomultiplier tube (PMT Hamamatsu R928) fitted with a 630 nm interference filter. The absorption due to atomic oxygen is calculated from the measured decay time of the photomultiplier signal. The oxygen atom density is corrected for the dead volumes between the active discharge zones and the mirrors (7 cm on each side). The homogeneity

of the plasma along the reactor length was verified with an axial scan of the optical emission intensities and showed variations of less than 8%. The temperature of the gas is determined from the Doppler broadening of the transition line profile.

Because of the principle of CRDS and the experimental setup used, the uncertainty of the CRDS measurement is very limited. No etaloning occurs as there are no optical elements between the surfaces of the two mirrors. The jitter of the tunable laser used is up to 0.001 cm^{-1}, but the laser position is continually monitored by the wavemeter with a precision of 10^{-5} cm^{-1}, preventing any effect on the accuracy of the temperature measurement. The statistical noise on the ringdown times leads to an uncertainty of the fits ($\pm 5\%$ on the density and $\pm$ 5 K on the temperature). The most significant uncertainty factors are the uncertainty of the transition strength and the estimation of the effective absorption path length. We calculated the transition strength from the Einstein A factor given by NIST, which is stated to have an estimated accuracy of B+, corresponding to $\leqslant 7\%$. However, this value results from a theoretical calculation, and has never been measured. Concerning the effective absorption length, diffusion calculations showed that the density of O atoms in the dead volume (between the plasma and the mirrors) was very low. We estimate that the uncertainties in the assumptions about the axial distribution of the O atoms add a further uncertainty of $\pm 3\%$ to the density measurements. Overall, the uncertainty on the O atom density measurements by CRDS is of $\pm 10\%$.

The CRDS technique requires sophisticated experimental hardware and critical alignment. The measurements are line-of-sight integrated, and thus depend on the homogeneity of the medium along the optical path, hindering its use in complex geometries. For these reasons, actinometry can be a good alternative for measuring atomic species.

4. Actinometry

4.1. Equations and principle

Actinometry relies on the comparison of the intensity of the emission from an excited state of the species of interest with that from a species whose density is known (the actinometer gas).

Assuming that excitation is dominated by single-step electron impact, the emission intensity of a line can be calculated from the product of the excitation rate and the radiative branching ratio. The intensity I_X of an emission line of species X between level i and level j at wavenumber ν is given by:

$$I_X = C_\nu \times h\nu_{ij}^X \times k_e^{X,i} \times n_e \times a_{ij}^X \times [X] \tag{3}$$

where ν_{ij} is the wavenumber of the transition, C_ν is the response coefficient of the observation device at wavenumber ν, $k_e^{X,i}$ is the rate coefficient of electron impact excitation from the ground state to level i, n_e the electron density, $[X]$ the density of species X and a_{ij}^X the effective branching ratio [6]. The relative spectral intensity sensitivity of the detection system, C_ν (from equation (3)) was determined using a reference tungsten lamp with known emission spectrum. The branching ratio, a_{ij}^X, represents the probability of radiative de-excitation through the observed line compared to all other deexcitation channels. The branching ratio can be written as:

$$a_{ij}^X = \frac{A_{ij}^X}{\sum A_i^X + \sum_Q k_Q^i [Q]} \tag{4}$$

where A_{ij} is the Einstein coefficient of transition $i \rightarrow j$, $\sum_i A_i$ is the sum of all Einstein coefficients of radiative transitions from level i, $[Q]$ is the density of species Q and k_Q^i is the collisional quenching coefficient of level i by species Q. The electron impact excitation rate coefficient, $k_e^{X,i}$, is given by:

$$k_e^{X,i} = \left(\frac{2e}{m}\right)^{1/2} \int_{\epsilon_{th}}^{\infty} \sigma_i^{\mathrm{exc}}(\epsilon) f(\epsilon) \sqrt{(\epsilon)} \mathrm{d}\epsilon \tag{5}$$

where $\sigma_i^{\mathrm{exc}}(\epsilon)$ is the excitation cross-section of level i, ϵ_{th} is the energy threshold of the cross-section, e is the electron charge, m is the electron mass and $f(\epsilon)$ is the EEDF.

If equation (3) is valid for both the species of interest and the actinometer, actinometry can be used. This means the excited level i must be populated predominantly by electron impact, and not dissociative excitation of a molecule, or by cascade from another state. Using an actinometer A radiating from i' to j', the density of species X can be obtained from the ratio of the two line intensities following equation (3):

$$[X] = \frac{I_X}{I_A} \frac{C_A}{C_X} \frac{h\nu_{i'j'}^A}{h\nu_{ij}^X} \frac{k_e^{A,i'}}{k_e^{X,i}} \frac{a_{i'j'}^A}{a_{ij}^X} [A]\,. \tag{6}$$

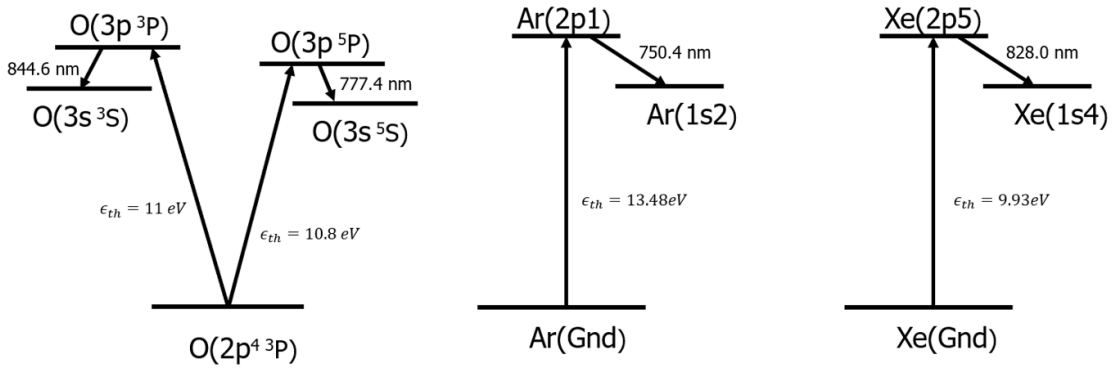

Figure 2. Atomic species levels used for O on Ar or Xe actinometry together with the respective transition lines used in the actinometry method developed in this work.

Ideally, the excitation cross-sections σ_i (of level i of species X) and $\sigma_{i'}$ (of level i' of the actinometer A) should have similar excitation thresholds (i.e $\epsilon_i \sim \epsilon_{i'}$ and $\sigma_i(\epsilon) \sim \sigma_{i'}(\epsilon)$) and shape to minimize the impact of inaccuracies in the computation of the EEDF.

Species A is usually a noble gas so that its density remains constant in the plasma, although some studies have used molecules from the plasma such as H_2 in [19].

4.2. Oxygen atom actinometry using Ar or Xe as the actinometer

The optical emission from O atoms in low-temperature plasmas is dominated by two intense lines: (1) a triplet (referred to as O777) centered around 777.4 nm (the three lines are very close and often unresolved, therefore no distinction is made between them), corresponding to the radiative deexcitation of O excited level $O(3p^5P)$ to level $O(3s^5S)$ [18], and (2) a second even more closely-spaced triplet (referred to as O845) centered around 844.63 nm corresponding to the deexcitation of level $O(3p^3P)$ to $O(3s^3S)$ [18]. The thresholds for excitation of the levels radiating the O777 and O845 lines are very close, respectively $\epsilon_{\mathrm{th}O(3p^5P)} = 10.8$ eV and $\epsilon_{\mathrm{th}O(3p^3P)} = 11$ eV, as shown on figure 2. Note that, the levels $O(3p^5P)$ radiating O777 and $O(3p^3P)$ radiating O845 can be populated not only by electronic impact on ground-state oxygen atoms, but also by other processes, including stepwise excitation via metastable states, cascades from higher excited levels and dissociative excitation of O_2. If the $O(^1D)$ or $O(^1S)$ metastable states of atomic oxygen are present in significant density, these can be further excited by electron collisions to the observed radiating states ($O(3p^3P)$ or $O(3p^5P)$). This stepwise mechanism was included in the collisional radiative model developed by Caplinger and Perram [20]. They found that, whereas it can be very significant at low pressures (1 mTorr), at 1 Torr the density of these intermediate states is strongly reduced by collisional quenching, this stepwise process becomes negligible compared to direct excitation (and cascades). This conclusion is supported by an experimental study of O_2 discharges by Germany *et al* [21], which showed that already at 20 mTorr there was no significant contribution from $O(^1D)$ to either of the radiating levels. Radiation trapping can occur if there is significant density in the lower levels of the observed transitions, namely $O(^3S_1^0)$ for O844 and $O(^5S_2^0)$ for O777. Caplinger and Perram [20] calculated the fractional population of these levels as a function of O_2 pressure, using a collision-radiation model of a pure O_2 discharge coupled to a Boltzmann solver. They assumed a constant effective electron temperature of 3 eV (with an LTE EEDF), slightly higher than those in our case, and an electron density of 10^{10} cm^{-3}. Their model indicates that the fractional density in the radiative $O(^3S_1^0)$ remains constant at the low value of about 3×10^{-9} until the pressure exceeds 100 Torr, at which point it becomes even lower due to collisional quenching. Although trapping of the resonant radiation at 130 nm from $O(^3S_1^0)$ to the ground state may affect this density, it is still far too low to cause trapping of O844. The density of the metastable $O(^5S_2^0)$ level was found to be significantly higher at low pressures. However, at 1 Torr, collisional quenching is already effective and the relative population is about 3×10^{-7}, corresponding (using our CRDS measurement of the total O density) to a density of about 10^6 cm^{-3} in this state. Over the 1 cm radius of the tube this can lead to about 10% absorption of the strongest component of the O777 triplet, or an escape factor close to unity (using the formula of the optical depth and the relationship between optical depth and escape factor provided in [22]). Caplinger and Perram [20] also calculated effective cascade cross-sections for the excitation of the $O(3p^3P)$ and $O(3p^5P)$ states. The cascade cross-sections for both levels is one order of magnitude lower than the direct excitation cross-section at 15 eV (corresponding to the far tail of the EEDF for our experimental conditions). Even

Table 2. Einstein coefficients and collisional quenching of the level used. All the A_{ij} are taken from the NIST database [18].

Level	Line	A_{ij} (s^{-1}) [18]	k_Q (m^3s^{-1})	
$O(3p^5P)$	777	3.69×10^7	10.6×10^{-16}	[27]
$O(3p^3P)$	844	3.22×10^7	9.4×10^{-16}	[7]
Ar $2p_1$	750	4.45×10^7	7.6×10^{-16}	[6]
Xe $2p_5$	828	3.69×10^7	9.8×10^{-16}	[28]

at the peak of the cascade cross-section for O844 (at 50 eV), it is only 1/3 of the direct excitation cross-section, in agreement with calculations of Julienne and Davis [23]. Therefore, cascade effects can be neglected under our conditions. The impact of dissociative excitation of O_2 on optical emission actinometry of oxygen atoms was investigated by Walkup *et al* [24]. Under their conditions (radiofrequency capacitive discharge at 390 mTorr) they found that this process can make a significant contribution to the O777 line, whereas the O844 line is much more immune to this effect, due to the higher energy threshold (20.5 eV compared to 17.5 eV) and smaller cross-section. This process can be included in equation 3. As discussed in previous works [6, 25], the dissociative excitation concerns only the $O(3p^5P)$ radiating O777 and can be included in equation (3). As a consequence, the intensity of the O777 line is given by

$$I_{O777} = C_{777} \times h\nu^O_{777} \times a^O_{777} \times n_e \times \left(k^O_e \times [O] + k_{de} \times [O_2]\right) \tag{7}$$

with k_{de} the dissociative excitation electron impact rate coefficient calculated from equation (5) and the corresponding cross-section. The cross-section in this case was taken from Schulman *et al* [26]. However, while dissociative excitation can be important in low-pressure discharges which have significant high-energy electron populations, it has been shown to be negligible in DC glow discharges at a few Torr in O_2 [4, 6]. The EEDF is indeed in local thermodynamic equilibrium, leading to a rapid decrease of the electron density in this high-energy region. Dissociative excitation is therefore negligible under our conditions compared to direct excitation from ground state atoms with lower energy thresholds. In this work, it was included for the intensity calculations but does not make a significant impact, accounting for less than 5% of the estimated oxygen density at most. We therefore chose to neglect it for the actinometry calculations.

For Argon, the 750.4 nm line is used. This corresponds to emission from $Ar(2p_1)$ ($4p'[\frac{1}{2}]_0$ in Racah notation) to $Ar(1s_2)$. This is the line that is customarily used in most studies when using Ar as an actinometer. The energy threshold of the excited level radiating 750 nm is $\epsilon_{thAr(2p_1)} = 13.48$ eV.

Although Ar is widely used in actinometry, it has some disadvantages, notably the low emission intensity, especially for low Ar percentages in the mixture. To avoid this inconvenience, as well as to check the results with a different actinometer gas, we also investigated the use of Xe. Xe is not commonly used because of its very high price, but has several advantages. First the emission line at 828 nm is very intense, so the signal is easily observed even for small percentages of Xe, minimizing the perturbation of the plasma. Secondly, the energy threshold of the excited level is closer to (indeed, lower than) that of O atoms, which in our conditions is closer to the bulk of the EEDF than the Ar threshold. This lower excitation threshold reduces the sensitivity to the errors in the tail of the EEDF, which are more challenging to calculate accurately than the bulk of the EEDF. The line used is the 828.2 nm line (referred to as the Xe828 line), which corresponds to radiation from the $2p_5$ level to the $1s_4$ level. The energy threshold of the $2p_5$ level is $\epsilon_{thXe(2p5)} = 9.82$ eV.

The spontaneous emission coefficients A_{ij} for all of these levels are taken from the NIST database [18] and are given in table 2, along with the collisional quenching coefficients and their sources. As shown in equation (4), in principle it is necessary to know the quenching coefficient for each excited state by each individual quencher present. However, these are not always available in the literature. Therefore we used the values for O_2 for all quenchers, using the approximation $\sum_q k_q n_q \sim k_{O_2} \times N$, with N being the gas density. This approximation has a limited effect, due to the low fraction of noble gas (and assuming that the O_2 dissociation fraction is small); it is supported by measurements of the collisional quenching rates in CO_2 and in O_2 in [6], which showed that quenching coefficients are quite similar for different molecular collision partners (such as CO_2 and O_2).

5. Challenges of actinometry

5.1. Inaccuracy of actinometry performed with commonly used cross sections

Previous comparisons of oxygen atom actinometry to other direct measurement methods have shown varying degrees of agreement. Pagnon *et al* [4], compared actinometry to VUV absorption spectrometry

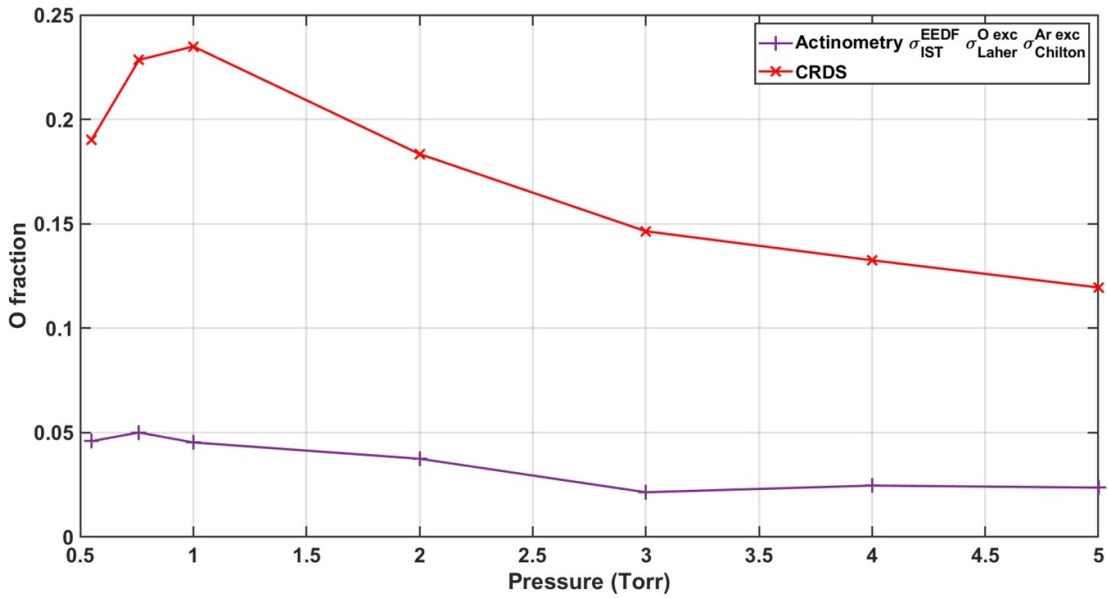

Figure 3. Comparison of O atom measurements taken simultaneously by CRDS and actinometry in a 95:5 O2:Ar low-pressure glow discharge at 40 mA. The CRDS results are plotted in red, and actinometry in purple. The excitation rate coefficient for oxygen atoms was calculated using the Laher cross-section [29], and that for Ar using the Chilton excitation cross-section [33].

in an O_2 glow discharge. The agreement was good: at 2 Torr, the [O]/[O_2] fraction was 0.19 with VUV absorption spectroscopy versus 0.22 for actinometry, giving credit to actinometry. A agreement was observed at the lower pressure of 0.36 Torr. However, a comparison of the O atom excitation cross-section shown in Pagnon *et al* [4], attributed to Laher and Gilmore [29] with the original cross-section from Laher and Gilmore [29] reveals a shift in the threshold for both O lines. The excellent agreement obtained by Pagnon *et al* [4] seems to depend on this threshold shift, a shift that is not justified or even discussed by the authors. Morillo-Candas *et al* [6], compared actinometry to TALIF in a CO_2 glow discharge. Actinometery indicated an oxygen fraction of 12%, while TALIF measured up to 19%, showing a 50% uncertainty on the [O]/N, which could be only partly attributed to the inaccuracy of the calibration procedure of TALIF by Xe [30].

Britun *et al* [31, 32] compared actinometry to TALIF in a pulsed radiofrequency discharge, but did not perform absolute calibration of the TALIF measurement. Rather, they simply normalized the TALIF measurements to O actinometry at one point. The TALIF and actinometry techniques showed similar trends, nevertheless a discrepancy of a factor 2 was seen at the beginning of the pulse.

An initial comparison of actinometry to CRDS in a low pressure O_2:Ar glow discharge is shown on figure 3. Here we used the O atom excitation cross-section proposed by Laher and Gilmore [29] to calculate the oxygen atom excitation rate coefficient, and the cross-section proposed by Chilton *et al* [33] for Ar. These cross-sections are among the most commonly used for actinometry [6]. In this first case we neglected the effect of the oxygen dissociation fraction on the EEDF calculation (the mixture is assumed to comprise only O_2 and Ar), as has been done in many previous studies. In this case, actinometry underestimates the O atom density by a factor close to 5 compared to CRDS. The question of the source of this discrepancy arises.

Using equation (7), the intensity of an emission line can be written as a function of basic collision data:

$$I_x = C_x \times h\nu^x_{ij} \times \left(\frac{2e}{m}\right)^{1/2} \int_{\epsilon_{th}}^{\infty} \sigma_i^{exc}(\epsilon) f\left(\epsilon, \sigma^{EEDF}\right) \epsilon d\epsilon n_e \times \frac{A^x_{ij}}{\sum A^x_i + \sum_Q k^x_Q [Q]} \times [X] \tag{8}$$

where $f(\epsilon, \sigma^{EEDF})$ is the EEDF and σ_i^{exc} is the electron impact excitation cross-section.

As discussed above, absorption measurements are a highly-reliable way to measure absolute densities. In contrast, actinometry, which relies on line intensity ratios, depends on a great number of basic physical data, obtained from measurements or theoretical calculations in the literature. The results of an actinometry measurement are therefore strongly influenced by uncertainties in the data used for the analysis. The most sensitive parameters for calculating properly individual line intensities are the following:

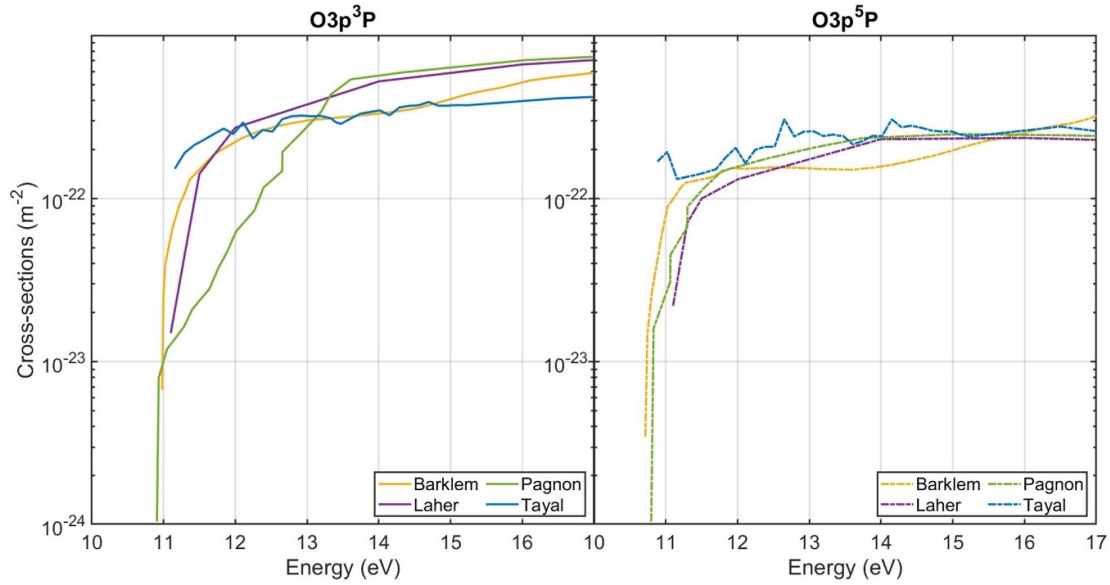

Figure 4. Excitation cross-sections used in this work for electronic excitation of oxygen to O($3p^3P$) (radiating O845) and O($3p5^P$) (radiating O777).

- the cross-section for electron impact excitation into each radiating level σ^{exc}
- the set of cross-sections used to compute the EEDF, σ^{EEDF}
- the quenching coefficients, k_Q.

These are discussed in the following sections.

5.2. The excitation cross-sections σ

Numerous energy-dependent excitation cross-sections for O, Ar and Xe levels are available in the literature. For oxygen atoms we consider four cross-sections proposed by Laher and Gilmore [29], Tayal and Zatsarinny [34], Barklem [35] and Pagnon *et al* [4]. These are compared in figure 4. They were digitized from the graphs in the respective papers, except for the case of Laher and Gilmore, where they are tabulated.

The first calculations of the cross-sections for the electronic excitation of O(^{3}P) to the excited states O(3p^{3}P) and O(3p^{5}P) were made by Julienne *et al* in 1976 [23] using the unitarized distorted wave method including exchange, described in [36]. A peak value of the direct excitation cross-section is given, as well as the cascade contributions from other levels.

The cross-sections proposed by Laher and Gilmore in 1990 in [29] were estimated from a review of the extant literature. They are based on the measurements of Gulcicek and Doering [37] (at 30 eV) and of Gulcicek *et al* [38], extended to more energies: 13.8 eV (close to the threshold), 20 eV, 50 eV and 100 eV. The values of Gulcicek *et al* [37, 38] are approximately 25% smaller than those given by Julienne and Davis [23]. Based on these measurements, the following approximation was proposed by Laher and Gilmore:

for $O\left(^3P \rightarrow 3p^5P\right)$	for $O\left(^3P \rightarrow 3p^3P\right)$
direct measurement from [38] $forE < 30\,\text{eV}$	direct measurement from [38] for $E < 100\,\text{eV}$
$\sigma(E) = 1.10 \times 10^{-16} \times E^{-1}$ for $E > 30\,\text{eV}$	$\sigma(E) = 1.81 \times 10^{-14} \times E^{-3}$ for $E > 100\,\text{eV}$

The cross-sections proposed by Laher and Gilmore contain more points than the measurements they are based on, therefore one must assume that the data was interpolated between the experimental points, and extrapolated down to the threshold energy (11 eV while the measurements start at 13.8 eV). However, the exact interpolation and extrapolation algorithms used are not given. For a glow discharge, whose bulk electron energy is at 2.5 eV, only electrons in the tail of the EEDF (with energies higher than 10 eV) are capable of exciting oxygen atoms. In this case, the shape of the cross-section above 15 eV is irrelevant, as very few electrons have that energy. Hence, the cross-sections of Laher and Gilmore, when applied to a low pressure glow discharge, are only supported by one experimental point, measured by Gulcicek and Doering at 13.8 eV [37].

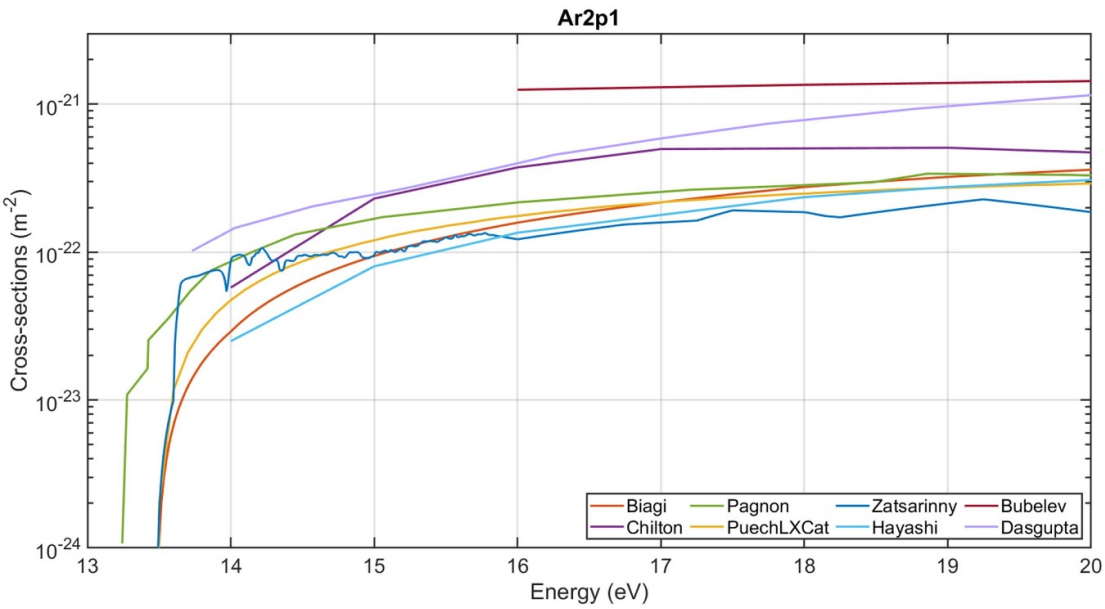

Figure 5. Excitation cross-sections used in this work for the electron impact excitation of Argon to the Ar(2p1) level.

The theoretical cross-section proposed by Barklem [35] is computed using a 38-state R-Matrix including L–S coupling, and was intended for the interpretation of emission spectra in astrophysics. It was compared to the measurements of Gulcicek *et al* [38], showing a large deviation (40%) with the point at 13.87 eV.

Tayal and Zatsarinny [34] more recently calculated cross-sections using the B-spline R (BSR) Matrix method between 11 and 200 eV. This result was compared to experimental measurements by Vaughan and Doering [39] and by Kanik *et al* [40]. However, these experiments provide only a limited number of points over the studied range (3 points for [39] and approximately 20 points for [40]), and with large uncertainties. The agreement between the calculated and experimental cross-sections must therefore be considered with caution.

The Laher and Gilmore (henceforth referred to as Laher) cross-section is, to date, the one most commonly used for O actinometry [6, 41] and for collisional radiative models of oxygen plasmas [20, 42]. It was the first theoretical and experimental review of O excitation, and gives data for numerous excitation processes, making it convenient for O atom radiative models. The Barklem and Tayal cross-sections are, however, much more recent and use more complete descriptions of the collision processes.

The fourth cross-section we consider is that of Pagnon *et al* [4]. Supposedly taken from Laher and Gilmore [29], a comparison between the two shows a clear shift of the electron energy axis. This difference could stem from the extraction of the cross-sections from figure 5 in [29]. Nevertheless, given the good results in terms of measured density given by Pagnon in [4], these cross-sections are worth investigating.

For Argon, we compare eight cross-sections for direct excitation to the $2p_1$ level : Chilton *et al* [33], Puech and Torchin [43], Zatsarinny *et al* [44], Hayashi [45], Bubelev and Grum–Grzhimailo [46], Dasgupta *et al* [47] and Pagnon *et al* [4]. They are plotted on figure 5. The cross-sections from Biagi, Chilton, Puech and Zatsarinny were taken from the LXCat database, as discussed by Pitchford *et al* [48].

The Biagi cross-section is taken from the Magboltz Fortran code developed by S.F.Biagi, which is a Monte Carlo code which calculates the trajectory of electrons in a magnetic and/or electric field. This data is available in the LXCat 'Magboltz 8.1' database.

The Zatsarinny cross-sections [44] were computed using the BSR-Matrix method with JK Coupling. They have been compared with experimental data [33, 49–51]. Relatively good agreement was found with the measurements of Chutjian and Cartwright [49], although some discrepancies lead the authors to question the absolute normalization accuracy. It is available on the LXCAT database (BSR500 database).

The Puech cross-section is taken from the 1986 compilation of cross-sections in Puech and Torchin [43]. The data are taken from various sources: the cross-sections for momentum transfer are from Frost and Phelps [52], and for inelastic processes (with thresholds above 20 eV) from a set developed by Bretagne *et al* [53], based on the measurements of Chutjian and Cartwright. For lower energies, the

set is based on measurements by Schaper and Scheibner [54]. The values used here are taken from the Puech database on LXCat .

The Ar cross-section given by Pagnon is supposedly the same that of Puech, drawn from [43]. The data shown was digitized from the article of Pagnon *et al* [4]

The Hayashi cross-section is given in the literature review of 2003 [45], which was a compilation of the available data on Ar excitation cross-sections. Data for elastic momentum transfer, electronic excitation and ionization of Ar is available. The reasons for the choices made are not discussed in the report, only the final recommendations are given. The data were again digitized from the graphs in this paper.

The Chilton *et al* cross-sections [33] were determined experimentally from 0 to 300 eV. All emissions in the range 650–1100 nm were measured by Fourier-transform spectroscopy, which allowed separation of cascade contributions from direct excitation. A previous measurement by Ballou *et al* [55] only estimated the cascade contribution. The cross-section is not well resolved around the excitation threshold, with its first point at only 14 eV. The Chilton cross-section is that used in the IST-Lisbon set for Ar, and is available on LXCat in the 'IST Lisbon' database.

The calculated cross-section of Bubelev and Grum–Grzhimailo [46] does not include the near-threshold region, but only starts at 16 eV, limiting the interest for our conditions. They compared their calculations to two previous calculations performed by Albat *et al* [56] using two different methods (plane-wave Born approximation PWBA and close-coupling calculations).; They found relatively good agreement (approximately 20% higher) at energies above 80 eV. However, significant disagreement was observed at lower energies. The calculated cross-sections were also compared to experimental values from Ballou *et al* [55], Chutjian and Cartwright [49] and Bogdanova [57]. An order of magnitude of difference was seen at low energies, reducing to a factor of 2 to 5 at higher energies. The authors underlined that the quality of the wavefunctions they used was unsure and stated that the validity of their calculations for that specific level could not be verified.

Dasgupta *et al* [47] calculated cross-sections using a modified distorted wave method. Specifically, the authors used ab-initio wave functions with full electron exchange and polarization of the outermost electron and proper conversion of the T matrix and R matrix. According to the authors, this modified method yields better results than the usual DW calculation, both near-threshold and at high energy, and allows the computation of electron impact excitation of the Ar from the ground state to the $2p_{1-10}$ states and to the $1s_{2-5}$ states. The data for $Ar2p_1$ excitation were compared to the simulated cross-sections of Bubelev and Grum–Grzhimailo [46] and Bartschat (from a private communication) as well as to the experimentally-measured cross-sections of Chutjian and Cartwright [49] and Chilton *et al* [33]. Near-threshold, the computed cross-section was in good agreement with the calculations of Zatsarinny, while it was in excellent agreement with the Bubelev cross-section above 50 eV. The cross-section from Dasgupta was, however, between 3 and 10 times higher than the experimental cross-sections. For this work, the cross section of Dasgupta was digitized from the source [47] and given in figure 5.

For the excitation of the $2p_5$ level of Xe we consider six cross-sections available in the literature: Biagi, TRINITI [58], Zatsarinny, Priti [59], Chiu *et al* [60] and Fons and Lin [61]. These are plotted on figure 6.

The Biagi cross-section was again taken from version 8.9 of the Magboltz Fortran code, as provided in LXCat as the Biagi database.

The TRINITI cross-sections (available in the TRINITI database on LXCat) were taken from Baranov [58], published in 1979.

The Xe cross-sections proposed by Zatsarinny are available in the BSR LXCat database. The cross-section for excitation to the Xe $2p_5$ level has not been published. However, Zatsarinny and Bartschat [62] published a benchmark of the BSR Matrix method, including several computed cross-sections for Xe excitation, and comparison of the results to experimental data. The excitation cross-sections to the $5p^5$ 6 s ($J = 0$, 2) and $5p^5$ 6 s ($J = 1$) levels were compared to the experimental data of Buckman *et al* [63] and found to be in relatively good agreement.

The Priti cross-sections [59] were calculated using the relativistic distorted wave theory. The results are of comparable magnitude to the BSR calculations at high energy ($\epsilon > 20$ eV) but show a strong disagreement near the threshold.

Fons and Lin [61] measured Xe excitation cross-sections using a beam of monoenergetic electrons generated by a heated cathode. The light emitted was then analysed by a monochromator and PMT. A theoretical treatment was used to extract the direct excitation cross-sections from the observed cross-sections (which include radiative cascades from other levels). However, the observed cross-section was highly sensitive to pressure.

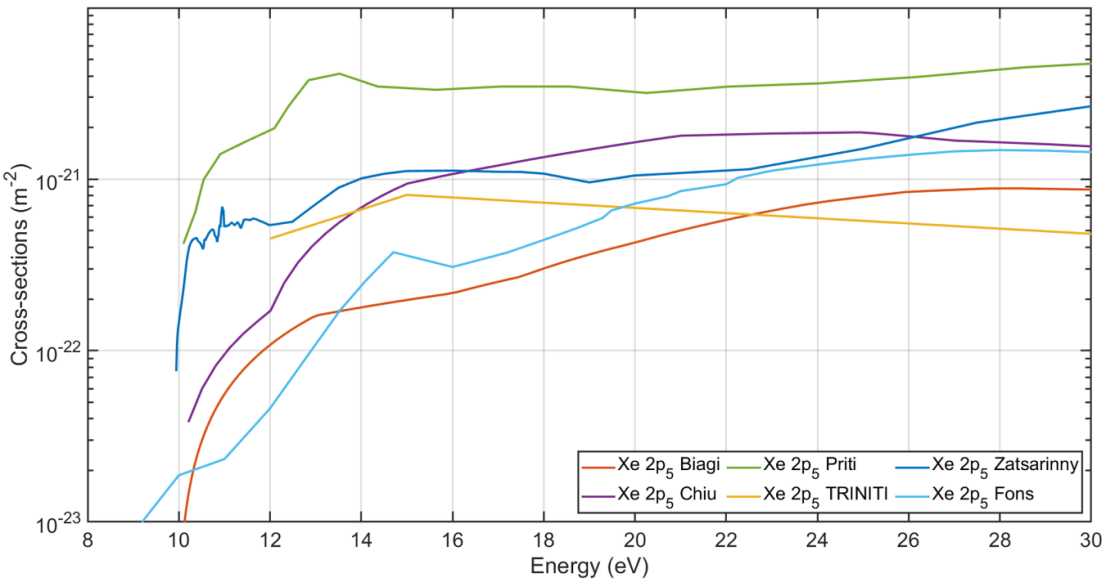

Figure 6. Excitation cross-sections used in this work for Xe $2p_5$.

Similarly, Chiu *et al* [60] measured the emission spectrum of a single-collision beam experiment for energies ranging from 10 to 70 eV. The measurements were compared to Fons and Lin [61] and were found to be in good agreement for most of the Xe $2p_i$ states

In the rest of this work, the excitation cross-sections for a specific level of a species X is denoted $\sigma^{X\,\mathrm{exc}}_{\mathrm{source}}$, *e.g* $\sigma^{\mathrm{O}\,\mathrm{exc}}_{\mathrm{Tayal}}$ for the O excitation cross-sections proposed by Tayal.

5.3. Cross section sets used to calculate the EEDF

In a DC glow discharge the EEDF can be calculated, for a given value of the reduced electric field, using a Boltzmann solver combined with a complete set of the elastic and inelastic cross-sections for the gas in question. Excitation rates can then be calculated from the EEDF and the excitation cross-sections. The actinometry proportionality constant can then be calculated from the ratio of the excitation rates for oxygen atoms and for rare-gas atoms. However, the result obtained is highly sensitive to the form of the EEDF, because the excitation threshold energies (∼10–13 eV) correspond to the tail of the EEDF for a glow discharge whose mean electron energy is around 2.5 eV. To our knowledge, the only complete and consistent set of cross-sections for O_2 electron impact publicly available is the one from the IST database, available on LXCat (referred to this as the 'IST set' in the rest of this work). This dataset was generated by the IST team by combining the cross-sections from Gousset *et al* [64], with estimations of the cross-sections for the remaining (unmeasured) processes. The shape and amplitudes of these additional cross-sections were adjusted until the calculated swarm parameters matched the measured ones. No other sets proposed in the literature are consistent with the measured swarm parameters. However, we will also consider the O_2 cross-section set proposed by Biagi from his code Magboltz. This set has a major drawback: the ionization coefficient is not well reproduced as a function of the electric field compared to available swarm measurements [65–67], which in this particular case is a problem, because the O_2 ionization threshold is around 11 eV, precisely where the O777 and O845 lines excitation take place. Overall, this means that the Biagi set is less likely to accurately reproduce the EEDF in this region. Apart from the reduced Townsend coefficient for the Biagi set, all other swarm parameters are well reproduced.

The same problem arises for the selection of cross-sections sets for the actinometer gases, i.e. Argon and Xenon. Although they represent at most 5% of the gas, they will have some effect on the EEDF calculation. Several sets are available in literature [68] and are given in the IST Lisbon database, [33, 43] for Ar and Xe [62, 69]. Here we only consider one set of cross-sections for Ar and for Xe, because the impact is expected to be limited for small rare gas additions. For Ar we chose the IST set [68], which has been validated against the swarm parameters. For Xe, the Biagi set [69] was used.

Finally, we must estimate the collision cross-sections for atomic oxygen, which can make up to 30% of the gas mixture. No set exists which has been validated against swarm parameters for mixtures of atoms and molecules, so the effect of oxygen atom cross-sections on the EEDF is challenging to evaluate.

For this work, the set of electron impact cross-section on atomic oxygen from the IST database was chosen for the EEDF calculation.

In the rest of this work, the set of O_2 cross-sections used for the computation of the EEDF is denoted $\sigma^{\text{EEDF}}_{\text{source}}$, *e.g* $\sigma^{\text{EEDF}}_{\text{IST}}$ when the EEDF set used is taken from the IST database.

5.4. The accuracy of the quenching coefficients

The calculations are also affected by the values of the quenching coefficients used, although for the gas pressure range considered here this is less critical than for the excitation cross-sections. The quenching rate constants reported in the literature vary by a factor 2: for example, the rate of quenching of $O(3p^3P)$ by O_2 given by Meller *et al* [70] is half of that given by Dagdigian *et al* [71] (respectively $3.7\times10^{-10}\text{cm}^3\text{s}^{-1}$ vs $7.8\times10^{-10}\text{cm}^3\text{s}^{-1}$). However, the Dagdigian value is close to that measured in TALIF experiments by Niemi *et al* [27] and by Morillo-Candas [6], therefore we use this value for the rest of this study. The influence of quenching increases with pressure, and therefore different choices could change the trends with pressure. However, a change by a factor of 10 in the quenching coefficient would be needed to cause a significant difference. This is unlikely, given the number of experimental measurements of these rates. The current values, despite their uncertainty, will not be changed. The values used in this work are given in table 2.

6. Line intensity simulations

Actinometry is a line ratio method, therefore it does not allow cross-sections to be tested individually. Testing the effect of the excitation cross-section, σ^{exc}, the sensitivity of the EEDF on σ^{EEDF}, and the choice of quenching coefficients, would lead to numerous combinations and possible error compensation. Therefore we will first assess the accuracy of the determination of the intensity of individual lines before applying it to line ratios in the actinometry technique. To test parameters one by one, an intensity calculation algorithm was developed. The principle is to calculate the absolute number of photons emitted for each transition of interest, using the experimentally measured atomic oxygen density, O_2 density and temperature (from CRDS measurement), and the electric field (from the potential of the tungsten pins). The simulated intensity can then be compared to that measured by the spectrometer. The algorithm is summarized in figure 7. The experimental conditions are used as input for the LisbOn KInetics Boltzmann solver (LoKI-B) [72, 73]. A set of cross-sections is provided for the computation of the EEDF, and excitation cross-sections are provided for the computation of the rate coefficients. The electron density is deduced from the discharge current, C (set in the experiment), and reduced mobility (computed by LoKI-B):

$$n_e = \frac{\frac{C}{\pi r^2}}{q \times E/N \times \mu_{\text{red}}} \tag{9}$$

where r the tube radius and μ_{red} is the reduced mobility ($\mu_{\text{red}} = \mu \times N$ where μ is the mobility).

Finally, using equation (3), the intensities are computed for the lines of interest. The simulated intensities are then compared to the experimental values. The 'best' cross-section is the one that minimizes the difference between experiment and simulation over the whole range of plasma conditions tested.

Absolute calibration of measured emission intensity is a challenging task, beyond the scope of this work. Instead, the experimental and simulated intensities are normalized to the value of the O777 line at 1 Torr. This way, two things can be compared at once: (1) the trend with pressure (i.e indirectly with varying E/N) for the O777 line, which tests the validity of the chosen excitation cross-section σ^{exc}, and (2) the consistency of the all the other emission lines with the O777 line. Indeed, if the normalization is done on the O777 line, the O845 line should match the simulation if the cross-sections are consistent for both levels.

6.1. Line intensities in pure oxygen plasmas

First, we will compare the simulated and measured intensities in a pure O_2 discharge (to avoid the influence of Ar or Xe on the EEDF calculation). The O_2 flow is set to 7.4 sccm and the current to 40 mA. In these conditions of pressure (0.5–5 Torr), the reduced electric field E/N varies between approximately 90 and 45 Td (see figure 9 in the second part of this work [12]). We investigated two sets of cross-sections for the EEDF computation σ^{EEDF}, and four cross-sections for excitation to the specific O levels, as shown in table 3. In all EEDF calculations, the same cross-section set (from IST-Lisbon) is used for atomic O. The influence of the excitation of oxygen molecules into the metastable $O_2(a)$ state is neglected in the EEDF calculations, although it has been seen experimentally that the fraction can reach 10% of the total

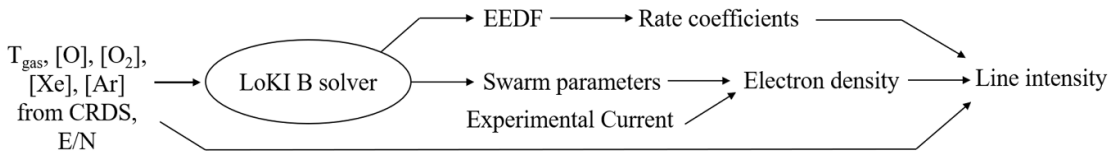

Figure 7. Principle of the absolute emission intensity computation.

Table 3. σ_{set}^{EEDF} and $\sigma^{O\,exc}$ tested for the comparison of the simulated and measured line intensity.

σ_{set}^{EEDF}	IST set, Biagi set
$\sigma^{O\,exc}$	Laher, Pagnon, Barklem, Tayal

O_2 density [74]. The influence of this state on the measurement of electric field by the line ratio method is discussed in the second part of this work [12]. In figure 8 the measured intensities of the two oxygen lines are compared to simulations using different O excitation cross-sections $\sigma^{O\,exc}$ but the same set (IST σ_{IST}^{EEDF}) for the computation of the EEDF. The data are normalized to the O777 value at 1 Torr. Note that the normalized measured intensity O845 at 1 Torr is (coincidentally) close to unity.

The intensities of both lines decrease monotonically with pressure in all cases. The decrease of the intensity with pressure occurs for several reasons. First, the reduced electric field decreases with increasing pressure (from 62 Td at 1 Torr to 47 Td at 5 Torr), leading to a significant reduction in the fraction of electrons with enough energy to excite the radiating levels. Secondly, collisional quenching increases with pressure. Finally, the fraction of atomic oxygen also decreases with pressure (except below 1 Torr). For the O777 line, all of the cross-sections, $\sigma^{O\,exc}$, considered give similar results. The value of the normalized experimental intensity reaches 1.16 at 0.5 Torr, close to the 1.24 reached in the simulation using the Tayal cross-sections $\sigma_{Tayal}^{O\,exc}$. The highest simulated value is obtained with the Laher cross-section $\sigma_{Laher}^{O\,exc}$, reaching 1.33. At 5 Torr, the experimental value drops to 0.24. The closest simulated value is 0.16, reached with the Tayal cross-section $\sigma_{Tayal}^{O\,exc}$, while the lowest value of 0.137 is again reached with the Laher cross-section $\sigma_{Laher}^{O\,exc}$. Overall, the best match for O777 is obtained with $\sigma_{Tayal}^{O\,exc}$, although the calculated results do not diverge greatly (this is partly explained by their normalization to the 1 Torr point). The results for the O845 line (normalized to the O777 emission at 1 Torr) are much more scattered. Here again, the simulation which best matches the experiment (*i.e* showing the smallest difference with the experiment over the whole pressure range) is obtained using the Tayal cross-section, most notably at 0.5 Torr (1.304 for the simulation vs 1.3 for the experiment), although the Pagnon cross-section also yields acceptable results. Using the Laher cross-section overestimates O844 by a factor of about 2 at all pressures, leading to the O844 line being more intense than the O777 line.

Now let us consider the effect of the cross-section set used to calculate the EEDF. Figure 9 shows the results of the same calculations as for figure 8, but using the Biagi set (instead of the IST set) for the EEDF computation (σ_{Biagi}^{EEDF}).

As before, the calculated O777 intensities are quite similar for all excitation cross-sections. The differences are again more visible for the O845 line. The best match is in this case obtained with the Pagnon cross-section, although the Tayal cross-section also gives a relatively good agreement with the experimental values.

For actinometry purposes, the cross-sections chosen ($\sigma^{EEDF} \times \sigma^{O\,exc}$) should be those that best predict the line intensity trends. The best combinations found so far are $\sigma_{IST}^{EEDF} \times \sigma_{Tayal}^{O\,exc}$, $\sigma_{IST}^{EEDF} \times \sigma_{Pagnon}^{O\,exc}$, $\sigma_{Biagi}^{EEDF} \times \sigma_{Tayal}^{O\,exc}$ and $\sigma_{Biagi}^{EEDF} \times \sigma_{Pagnon}^{O\,exc}$. Given the under-estimation of the ionization coefficient when using the Biagi set for the EEDF, and the aforementioned threshold problem of the Pagnon cross-section, the chosen combination is

$$\sigma_{IST}^{EEDF} \times \sigma_{Tayal}^{O\,exc}.$$

6.2. Line intensities in O_2 -Ar plasmas

Next we will investigate the effect of using different Ar excitation cross-sections. In figure 10 the variation with pressure (at 40 mA) of the experimental intensities Ar750, O777 and O845 are compared to simulations using the different $\sigma^{Ar\,exc}$ detailed in section 5.2. In all cases the EEDF is calculated using σ_{IST}^{EEDF}, and $\sigma_{Tayal}^{O\,exc}$ for O excitation. The cross-sections tested are summarized in table 4.

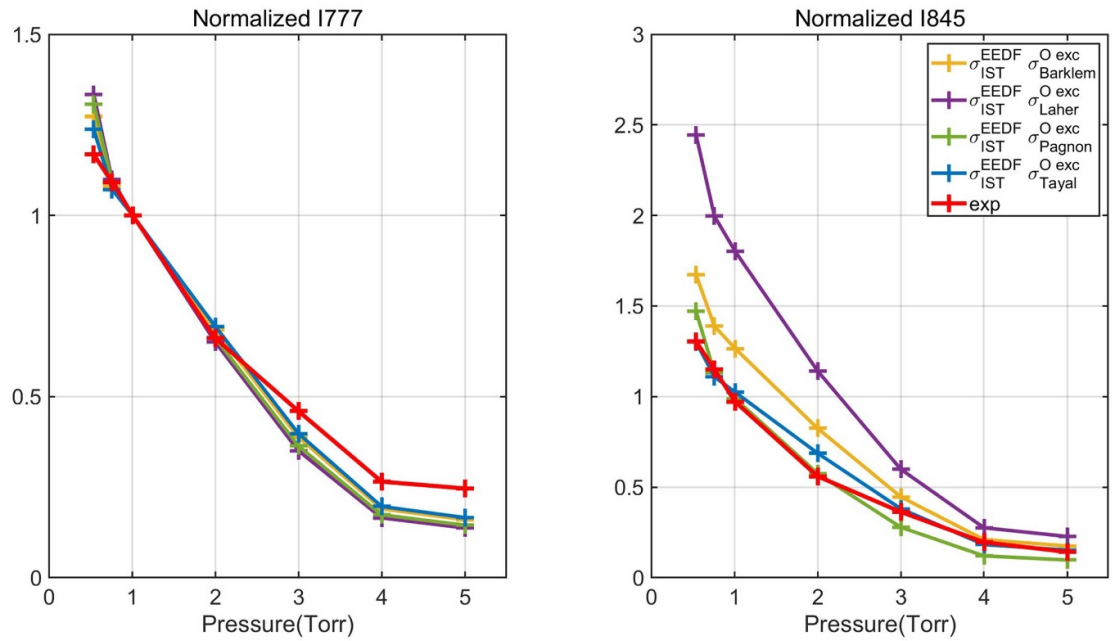

Figure 8. Trends of the O777 and O845 lines (normalized to the O777 emission at 1 Torr) as function of pressure: comparison of experiment (in red) to simulations using different $\sigma^{\mathrm{O\,exc}}$. The IST set ($\sigma^{\mathrm{EEDF}}_{\mathrm{IST}}$) is used for the computation of the EEDF. The current is set to 40 mA and the flow to 7.4 sccm.

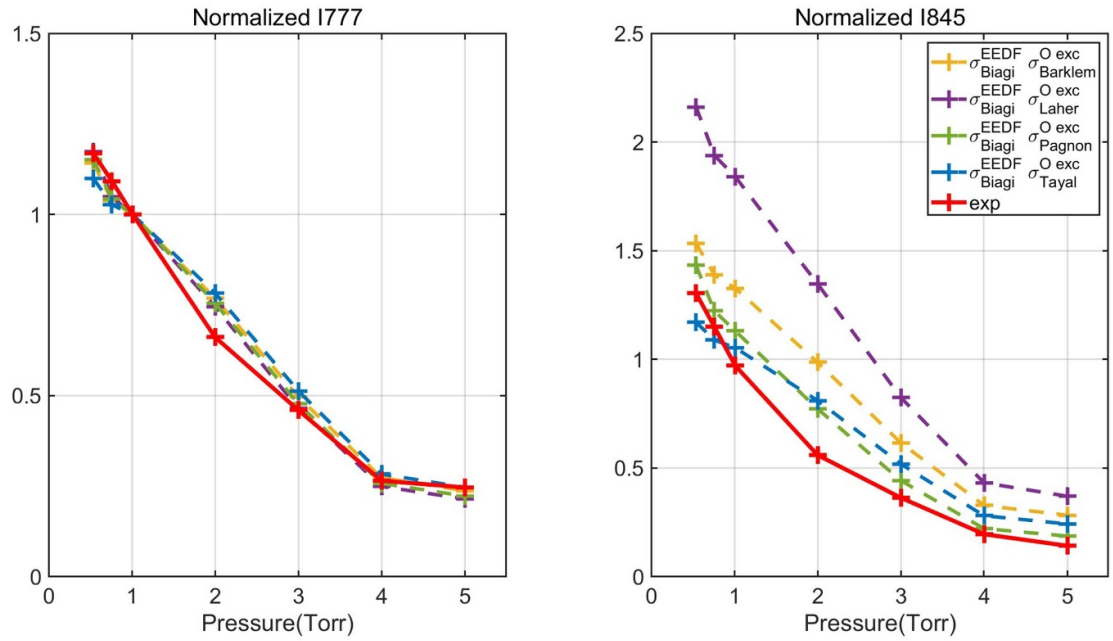

Figure 9. Pressure trends of the O777 line and O845 lines (normalized to the O777 emission at 1 Torr); comparison of experiment to simulations using different $\sigma^{\mathrm{O\,exc}}$. Same conditions as for figure 8, except the EEDF is calculated using the Biagi set ($\sigma^{\mathrm{EEDF}}_{\mathrm{Biagi}}$). The current is set to 40 mA and the flow to 7.4 sccm.

The O777 and O845 lines behave similarly to before, except that there is a slight drop in the oxygen line intensities at pressures below 1 Torr. This effect has been observed previously [74], where a drop in O density was observed below 1 Torr, attributed to an increase in the surface recombination probability caused by energetic ion bombardment. Interestingly, a comparison to the results in pure oxygen (figure 9) shows that this effect does not occur in pure O_2, but occurs with a small fraction of argon. In contrast, the Ar750 intensities decrease monotonically with pressure for all Ar cross-sections, due to the decreasing E/N and the increase of collisional quenching.

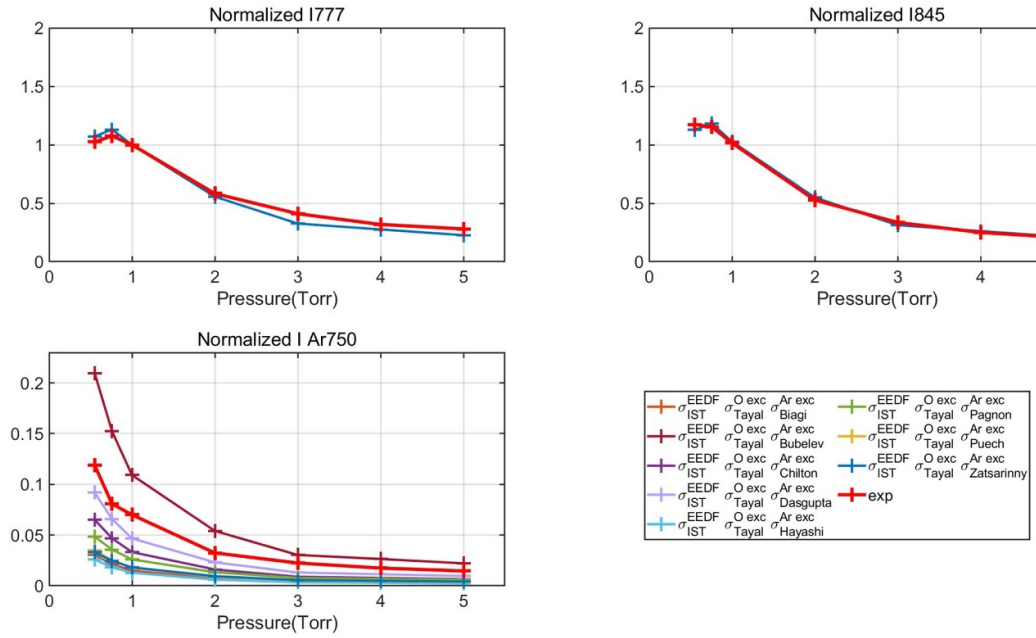

Figure 10. Variation of the Ar750, O777 and O845 lines as a function of pressure in a 95:5 O_2:Ar mixture at 40 mA. Comparison of the experimental measurements (in red) to simulations using different Ar excitation cross-sections. In all cases the IST set $\sigma^{\mathrm{EEDF}}_{\mathrm{IST}}$ was used for the computation of the EEDF, and the Tayal cross-sections $\sigma^{\mathrm{O\,exc}}_{\mathrm{Tayal}}$ for oxygen atom excitation. The lines are normalized to the O777 line at 1 Torr.

Table 4. $\sigma^{\mathrm{Ar\,exc}}$ tested for the comparison of the simulated and measured line intensity.

$\sigma^{\mathrm{EEDF}}_{\mathrm{set}}$	IST set
$\sigma^{\mathrm{O\,exc}}$	Tayal
$\sigma^{\mathrm{Ar\,exc}}$	Zatsarinny, Pagnon, Chilton, Puech, Biagi, Hayashi, Bublev, Dasgupta

For all $\sigma^{\mathrm{Ar\,exc}}$ (except for Bubelev) the simulated intensities are lower than the experimental measurement. The best agreement across the pressure range is given by the Dasgupta cross-section. At 0.5 Torr, the experimental value is 0.118 , while the simulated value using the Dasgupta cross-section reaches 0.092. At 5 Torr, the simulated value using the Dasgupta cross-section is 0.0095, close to the value (0.0145) measured experimentally. This does not mean that the Dasgupta cross-section is the most correct value; rather that over the electron energy range studied here, the Dasgupta cross-section for $Ar2p_1$ is the most consistent with the ones of Tayal for electronic excitation of the oxygen $3p^3P$ and $3p^5P$ levels, resulting in the most correct actinometry results. However, despite giving different absolute intensities, all of the cross-sections give reasonable predictions of the pressure trend of the Ar line intensity. The Zatsarinny cross-section in particular exhibits a very similar pressure trend to the experimental one, meaning that it would agree well with the measurements (over the whole pressure range) if multiplied by a constant factor of 3.0±0.2. This constant factor is further verified in the second part of this work [12]. Indeed because Zatsarinny *et al* also provide cross-sections for Xe calculated using the same method, it is worth studying further, especially for the line ratio method for the determination of the electric field using Ar and Xe (discussed in the second part of this work [12]). Hence, the two combinations chosen are:

$$\sigma^{\mathrm{EEDF}}_{\mathrm{IST}} \times \sigma^{\mathrm{O\,exc}}_{\mathrm{Tayal}} \times \sigma^{\mathrm{Ar\,exc}}_{\mathrm{Zatsarinny}}$$

for relative trend only

$$\sigma^{\mathrm{EEDF}}_{\mathrm{IST}} \times \sigma^{\mathrm{O\,exc}}_{\mathrm{Tayal}} \times \sigma^{\mathrm{Ar\,exc}}_{\mathrm{Dasgupta}}$$

for relative trend and best approximation of the absolute density

6.3. Line intensities in O_2 -Xe plasmas

Next we will investigate the best choice of cross-section for Xe excitation, using the same approach as was used for Ar. As before, we used the IST set $\sigma^{\mathrm{EEDF}}_{\mathrm{IST}}$ to compute the EEDF, and the Tayal cross-sections

Table 5. $\sigma^{\text{Xe exc}}$ tested for the comparison of the simulated and measured line intensity.

σ^{EEDFset}	IST set
$\sigma^{\text{O exc}}$	Tayal
$\sigma^{\text{Xe exc}}$	Biagi, Chiu, Fons Priti, TRINITI, Zatsarinny

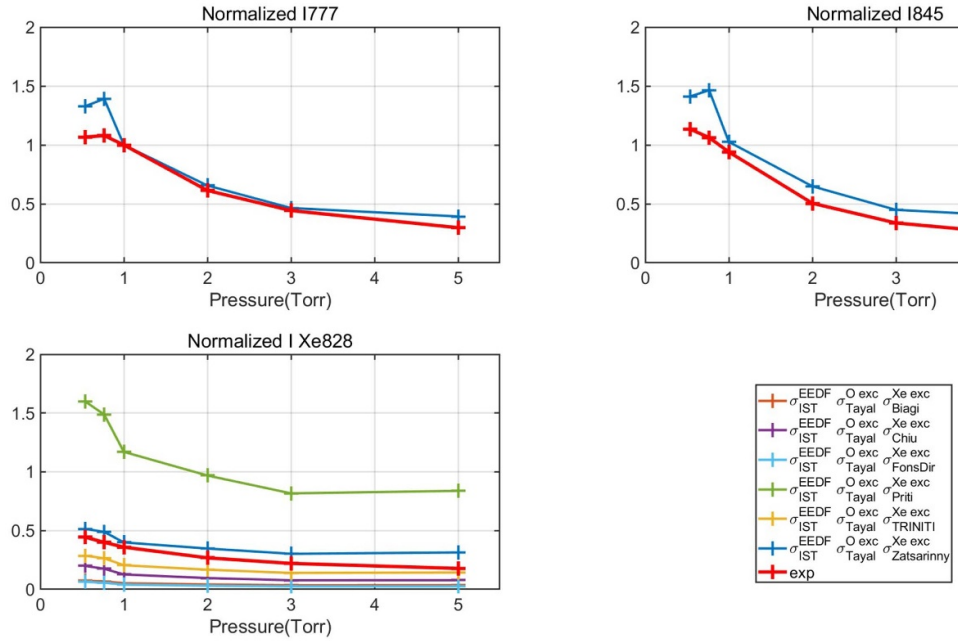

Figure 11. Pressure variation of the O777, O845 and Xe828 intensities in a 95:5 O_2:Xe mixture at 40mA: comparison of experiment (red) to simulations using different Xe excitation cross-sections . The lines are normalized to the O777 intensity at 1 Torr. The EEDF is calculated using the IST set $\sigma^{\text{EEDF}}_{\text{IST}}$, and the Tayal cross-sections $\sigma^{\text{O exc}}_{\text{Tayal}}$ were used for O atom excitation.

$\sigma^{\text{O exc}}_{\text{Tayal}}$ for oxygen atom excitation. The different cross-sections compared for Xe excitation are detailed in table 5.

The variation of the O777, O845 and Xe828 intensities as a function of pressure is plotted on figure 11. The experimental results (in red) are compared to simulations using different $\sigma^{\text{Xe exc}}$.

The experimentally observed Xe828 intensity (solid red line) drops from 0.44 at 0.5 Torr to 0.17 at 5 Torr. The calculated Xe828 intensities show much larger differences due to the wide spread between the different Xe excitation cross-sections, $\sigma^{\text{Xe exc}}$. The Priti cross-section $\sigma^{\text{Xe exc}}_{\text{Priti}}$ significantly overestimates the line intensity (by a factor 3 to 4). The best match is obtained with $\sigma^{\text{Xe exc}}_{\text{Zatsarinny}}$, with 0.51 at 0.5 Torr and 0.31 at 5 Torr. The TRINITI cross-section ($\sigma^{\text{Xe exc}}_{\text{TRINITI}}$) shows a very good agreement (0.18) at 5 Torr, but gives a substantial underestimate at lower pressure. The Fons, Chiu (the only measured cross-sections) and Biagi cross-sections all give poor agreement with the experiment. Overall, the combination of cross sections which gives the best individual line intensity calculation over the E/N range [45–90 Td] is the following:

$$\sigma^{\text{EEDF}}_{\text{IST}} \times \sigma^{\text{O exc}}_{\text{Tayal}} \times \sigma^{\text{Xe exc}}_{\text{Zastarinny}}.$$

7. Actinometry measurements

After an analysis of the factors influencing the intensities of individual O, Ar and Xe lines (and selection of a 'best working combination of base data'), we will now look at line ratios, i.e. the actual actinometry method. Calculations of the actinometric line ratios using the 'real mixture' (*i.e* with the O atom densities as measured by CRDS) to calculate the EEDF were compared to calculations assuming only pure O_2, and were found to yield better agreement with the CRDS measurements. An iterative algorithm was thus developed to account for the effect of O_2 dissociation on the actinometry calculations. The methodology is represented in figure 12. First, for a given discharge condition (pressure, input gas mixture, current), the gas temperature and reduced electric field are taken from the experimental measurements and an atomic oxygen fraction is assumed. From this, the O, O_2, Ar (and/or Xe) fractions can be computed. We then calculate the EEDF (using the Boltzmann solver LoKI-B), and then the excitation rate coefficients.

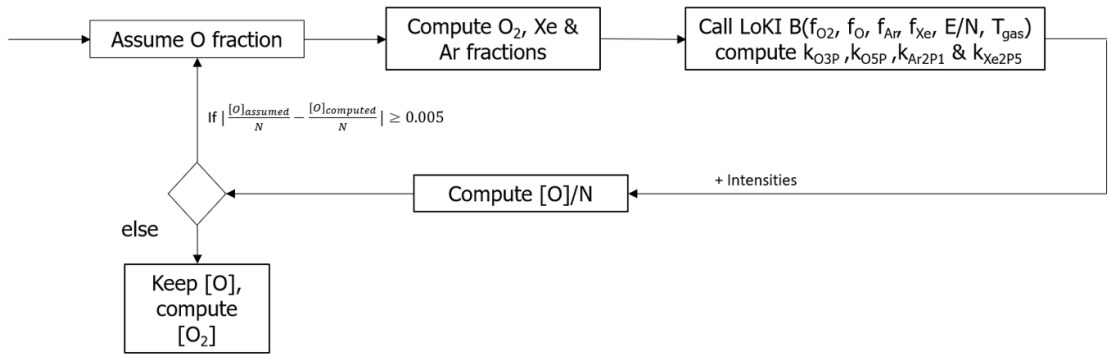

Figure 12. Principle of the actinometry algorithm.

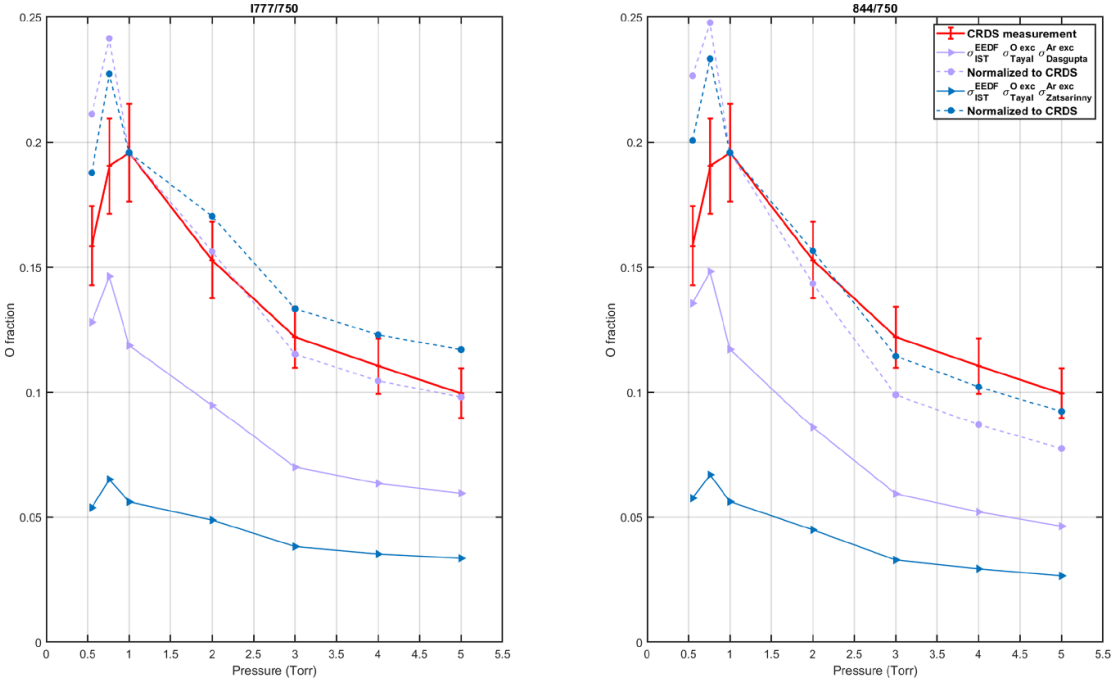

Figure 13. Comparison of the atomic O fraction in the plasma as a function of pressure determined by CRDS (plain red line) and by Actinometry, using Ar as the actinometer. The dashed lines with round markers are the results obtained with $\sigma^{\mathrm{O\,exc}}_{\mathrm{Tayal}} \times \sigma^{\mathrm{Ar\,exc}}_{\mathrm{Dasgupta}}$ and $\sigma^{\mathrm{O\,exc}}_{\mathrm{Tayal}} \times \sigma^{Ar\,exc}_{\mathrm{Zatsarinny}}$ normalized to the 1 Torr point of the CRDS, respectively in purple and blue.

These are then used with the observed intensity ratio, the Einstein coefficients and the quenching coefficients (given in table 2) to estimate the O fraction in the plasma. This value is then compared to the input atomic oxygen fraction. If the difference exceeds 0.5% of the gas density, the estimated O fraction is used as the new input oxygen fraction and the algorithm is iterated. If the assumed and computed O fractions converge, this value is kept as the actinometric result. In this section we present a direct comparison of CRDS and actinometry measurements in a glow discharge at 40 mA for two mixtures: 95:5 O_2:Ar and 98:2 O_2:Xe. Measurements in the ternary mixture O_2:Ar:Xe (both pressure and current trends) are presented in the second part of this work [12] and confirm the results presented here.

7.1. Actinometry in O_2-Ar mixtures

Figure 13 compares the O fraction in the discharge estimated by actinometry to that determined by CRDS. The left panel shows the results obtained using the O777 line and the right panel the results obtained with the O845 line. The CRDS points are plotted in red.

The actinometry results (obtained using the optimal cross-sections as previously discussed), $\sigma^{\mathrm{O\,exc}}_{\mathrm{Tayal}} \times \sigma^{\mathrm{Ar\,exc}}_{\mathrm{Zatsarinny}}$ and $\sigma^{\mathrm{O\,exc}}_{\mathrm{Tayal}} \times \sigma^{\mathrm{Ar\,exc}}_{\mathrm{Dasgupta}}$, are plotted with solid lines and triangle markers. For clarity, no other combinations of cross-sections are shown; we have demonstrated above that the results were not as good as those obtained with the presented combinations.

In all cases, the values obtained by actinometry severely underestimate the oxygen atom mole-fraction. Considering actinometry using the O777 line, it appears that the best match is obtained using the Dasgupta cross-sections for Ar, as expected from the single line intensity analysis above. The combination $\sigma^{\mathrm{O\,exc}}_{\mathrm{Tayal}} \times \sigma^{\mathrm{Ar\,exc}}_{\mathrm{Dasgupta}}$ yields the best results in terms of absolute values, approximately half of the CRDS measurement. At 0.5 Torr, the actinometry measurement using $\sigma^{\mathrm{O\,exc}}_{\mathrm{Tayal}} \times \sigma^{\mathrm{Ar\,exc}}_{\mathrm{Dasgupta}}$ yields an O fraction of 0.116, lower (by a factor 0.6) compared to the value of 0.185 measured with CRDS. This ratio remains the same at pressures between 1 and 4 Torr. The difference becomes smaller at 5 Torr, with 7.5×10^{-2} for actinometry and 10×10^{-2} for CRDS. The results are similar for the O845 line. The results obtained with the combination $\sigma^{\mathrm{O\,exc}}_{\mathrm{Tayal}} \times \sigma^{\mathrm{Ar\,exc}}_{\mathrm{Dasgupta}}$ are still approximately 0.6 times lower than the CRDS measurements between 1 and 5 Torr.

In order to see if the trends in oxygen atom mole-fraction are well-represented by actinometry (even if the absolute values are wrong), the actinometry results normalized to the CRDS-measured O fraction at 1 Torr are also plotted in figure 13(dashed lines with round markers).

Using both lines, the combination $\sigma^{\mathrm{O\,exc}}_{\mathrm{Tayal}} \times \sigma^{\mathrm{Ar\,exc}}_{\mathrm{Zatsarinny}}$ gives the best trend (as seen with the round markers), but the trend obtained with the $\sigma^{\mathrm{O\,exc}}_{\mathrm{Tayal}} \times \sigma^{\mathrm{Ar\,exc}}_{\mathrm{Dasgupta}}$ is also very close . Over this pressure range, the trends obtained with both the $\sigma^{\mathrm{O\,exc}}_{\mathrm{Tayal}} \times \sigma^{\mathrm{Ar\,exc}}_{\mathrm{Zatsarinny}}$ and the $\sigma^{\mathrm{O\,exc}}_{\mathrm{Tayal}} \times \sigma^{\mathrm{Ar\,exc}}_{\mathrm{Dasgupta}}$ are reasonably good, meaning that a constant factor (of 1.7 for Dasgupta and 3.0 for Zatsarinny) could be used to match the actinometry results to the CRDS measurements, as discussed previously.

In the second part of this work [12], it is shown that, over the range of pressures studied here, the same correction factor for the Ar excitation cross-section $\sigma^{\mathrm{Ar\,exc}}_{\mathrm{Zatsarinny}}$ (a correction factor of 3.0±0.2) can be used to perform both actinometry and E field measurements via a line ratio method, in good agreement with other measurement techniques, which reinforces the idea that this correction factor is accurate.

It is important to note that, even without this correction, actinometry gives a reasonable measurement of the relative variation with pressure of the O atom fraction, and the absolute oxygen atom density is correct to better than an order of magnitude.

It must be pointed that the values obtained at low pressure (0.5 and 0.75 Torr) are not aligned with the rest of the points (when normalized to CRDS at 1 Torr). The peak of the O atom fraction is seen at lower pressure for actinometry (0.75 Torr) compared to CRDS (1 Torr). This could be due to the uncertainty in the shape of the cross-section. The low-pressure points correspond to higher reduced electric fields (approximately 50 Td at 5 Torr, 60 Td at 1 Torr and 90 Td at 0.5 Torr). At higher pressure, the integral $\int_{\epsilon_{\mathrm{th}}}^{\infty} \sigma_i^{\mathrm{exc}}(\epsilon) f(\epsilon) \epsilon \mathrm{d}\epsilon$ is mostly sensitive to the near-threshold area of the Ar excitation cross-section, *i.e* close to 13.48 eV. At lower pressures the reduced electric field is higher, and the integral becomes more sensitive to the higher-energy part of the excitation cross-sections. In the case of Ar (figure 5) the cross-section shows substantial oscillations in this region. This could explain the observed difference at low pressure between CRDS and actinometry.

7.2. Actinometry in O_2-Xe mixtures

A comparison between CRDS and actinometry using Xe as actinometer is shown in figure 14. The CRDS-measured mole-fraction is plotted in red. In this case, several actinometry results using different Xe excitation cross-sections are plotted as solid lines. Because the results obtained with Xe are closer to the CRDS, no results normalized to CRDS are plotted. The results using the O777 line are plotted on the left panel and the results with the O845 line are plotted on the right. For both emission lines, the best match between CRDS and actinometry is clearly obtained with the combination $\sigma^{\mathrm{O\,exc}}_{\mathrm{Tayal}} \times \sigma^{\mathrm{Xe\,exc}}_{\mathrm{Zatsarinny}}$. For the O777 line at 0.5 Torr, the O fraction obtained using the $\sigma^{\mathrm{O\,exc}}_{\mathrm{Tayal}} \times \sigma^{\mathrm{Xe\,exc}}_{\mathrm{Zatsarinny}}$ is in excellent agreement with CRDS (19.9% for actinometry vs 20.5% for CRDS). At 1 Torr, the actinometry using this combination yields an O fraction of 22.1%, quite close to the 24.85% measured with CRDS. The difference increases at 5 Torr (18.8% for actinometry vs 13.9% for CRDS). The TRINITI cross-section $\sigma^{\mathrm{Xe\,exc}}_{\mathrm{TRINITI}}$, which gave good predictions of the Xe intensities, when used for actinometry give less good agreement with the CRDS measurements.

For the O845 line, the actinometry measurements using the $\sigma^{\mathrm{O\,exc}}_{\mathrm{Tayal}} \times \sigma^{\mathrm{Xe\,exc}}_{\mathrm{Zatsarinny}}$ combination are in excellent agreement with the CRDS measurements. At 0.5 Torr, the O fraction measured with actinometry is 19.3%, only about 1% away from the 20.5% of O atoms measured with CRDS. The largest difference is observed at 0.75 Torr but there is only an error of 2% on the absolute density (21% for actinometry vs 23.3% for CRDS). Above 1 Torr, the largest difference between CRDS and actinometry is 0.38% and is obtained at 3 Torr (16.4% with CRDS vs 16.8% with actinometry). Here again, the best results are obtained with O845 line.

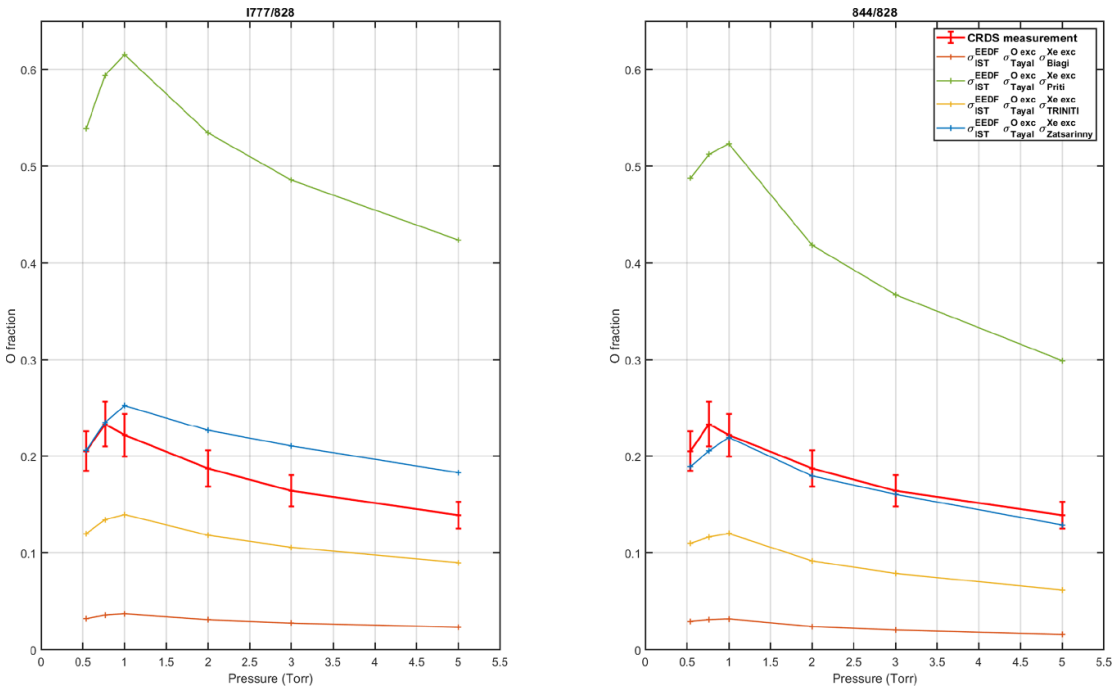

Figure 14. Comparison of the measurement of the atomic O fraction in the plasma as a function of pressure with CRDS (plain red line) and Actinometry, using Xe as an actinometer.

Two details should be noted. First, the peak of O atom density is once again shifted in the actinometry measurements compared to CRDS (0.75 Torr in CRDS, 1 Torr in actinometry). The shift is in the opposite direction compared to the Ar case (where the peak of O atom was detected at 0.75 Torr with actinometry and at 1 Torr with CRDS). This could again be due to the shape of the cross-section, or to uncertainty in the computation of the EEDF (originating from errors in the complete cross-section set). Although the origin of this inconsistency is unclear, the difference remains small and the actinometry technique nevertheless shows the decrease of O atom density below 0.75 Torr. Second, the TRINITI excitation cross-section for Xe, which yielded promising results in terms of line intensities, is quite far off for actinometry, while the Zatsarinny cross-section gives excellent results for actinometry but only good results for line intensities. This suggests that there is error compensation in the ratios used for actinometry. It is clearly visible on figure 11 that the O845 intensity using $\sigma^{\mathrm{O\,exc}}_{\mathrm{Tayal}}$ (on the upper right panel) and that the Xe828 intensity using the $\sigma^{\mathrm{Xe\,exc}}_{\mathrm{Zatsarinny}}$ (on the lower left panel) exhibit the same trend, *i.e* are slightly above the experimentally measured intensity. These similar trends compensate when using actinometry. On the contrary, the Xe828 intensity calculated using $\sigma^{\mathrm{Xe\,exc}}_{\mathrm{Triniti}}$ is slightly below the experimental measurement on figure 11. This error is increased when taking ratios. This could be made even more visible by normalizing all points to the emission of the O845 line at 1 Torr. The result using the TRINITI cross-section would then appear further from the experimental points that it does when normalized to the O777 line. The TRINITI cross-section for Xe is therefore not a 'bad' cross-section, but it is not the best suited for actinometry when combined with the Tayal cross-section for O.

8. Conclusions

Actinometry is a simple but powerful technique which can easily yield a fair approximation of absolute atomic densities and their trends with discharge parameters. This, however, requires the use of adequately accurate collision data. An analysis of the suitability of the available collision data was conducted by comparing line intensity calculations to measurements in a low pressure DC glow discharge at a few Torr in O_2–Ar and O_2–Xe mixtures. In this system the absolute O atom density and gas temperature was measured by CRDS, and electric field was measured directly by floating probes. A line intensity simulation algorithm was built, and compared to the experimentally measured plasma emission intensities. In this way we have been able to examine the consistency of 4 O atom, 8 Ar atom and 6 Xe atom excitation cross-sections. The 'best' combinations of total cross-sections set (for EEDF calculation) and atomic excitation cross-sections were identified and tested for actinometry. The actinometry measurements were compared with O fraction measured by CRDS.

To perform actinometry measurements yielding accurate trends and fair approximations of the O atom density, we recommend using the IST set of cross-sections to compute the EEDF [64], the Tayal cross-sections for the excitation of O atoms to the $3p^3P$ and $3p^5P$ levels [34], and the Dasgupta cross-section [47] for the excitation of Ar to the $2p_1$ level. Using this combination allows reasonable results to be obtained without any correction. We also recommend allowing for feedstock dissociation (O atom fraction) in the computation of the EEDF via a self-consistent calculation (as described in section 7).

To increase the accuracy of the O atom density measurement by actinometry, the cross-section proposed by Zatsarinny [62] for the excitation of Ar to the $2p_1$ level can also be used, multiplied by a correction factor of 3, as discussed in the second part of this work [12]. This correction factor could seem a little arbitrary if it were based solely on this comparison with oxygen density values. In order to verify the robustness of the correction proposed here, it is necessary to find another way to test it. This is done in the second part of this study [12], where the validity of the correction factor is assessed by calculating the electric field determined from the ratio of Ar and Xe lines. As for the actinometry using Xe as actinometer, we recommend using the IST set of cross-sections to compute the EEDF [64], the Tayal cross-sections for the excitation of O atoms to the $3p^3P$ and $3p^5P$ levels [34], and the Zatsarinny cross-section for the excitation of Xe to the $2p_5$ level, which allows to obtain both good absolute values of the oxygen density and correct trends of the evolution of the density along the reduced electric field. Beyond this correction factor for the Zatsarinny cross-section, the set of cross-sections studied here and the corresponding conclusions about the most suitable choice of cross-sections for actinometry analysis will also be rediscussed in [12] in the light of the reduced electric field comparisons.

Data availability statement

The data cannot be made publicly available upon publication because the cost of preparing, depositing and hosting the data would be prohibitive within the terms of this research project. The data that support the findings of this study are available upon reasonable request from the authors.

Acknowledgments

IPFN activities were funded by FCT (Fundaçao para a Ciencia e a Tecnologia) under projects UIDB/50010/2020 (https://doi.org/10.54499/UIDB/50010/2020), UIDP/ 50010/ 2020 (https://doi.org/10.54499/UIDP/50010/2020), LA/ P/ 0061/ 2020 (https://doi.org/10.54499/LA/P/0061/2020) and PTDC/ FIS-PLA/ 1616/ 2021 (https://doi.org/10.54499/PTDC/FIS-PLA/1616/2021).

ORCID iDs

E Baratte 0009-0009-8783-3446
L Kuijpers 0009-0000-6369-3674
T Silva 0000-0001-9046-958X
V Guerra 0000-0002-6878-6850
M C M van de Sanden 0000-0002-4119-9971
J-P Booth 0000-0002-0980-3278
O Guaitella 0000-0002-6509-6934

References

[1] Coburn J W 1986 Summary abstract: diagnostics in plasma processing *J. Vac. Sci. Technol. A* **4** 1830–2
[2] Chen C, Hong T and Chen S 1993 Role of hydrogen and oxygen in diamond synthesis using carbon-dioxide-methane-gas mixtures *J. Appl. Phys.* **74** 4483–9
[3] Ricard A, Henriques J, Cousty S, Villeger S and Amorim J 2007 Determination of n-, h- and o-atom densities in N2-H2 and in N2-O2 gas mixtures by optical actinometry in flowing microwave discharges and by no titration in post-discharges *Plasma Process. Polym.* **4** S965–8
[4] Pagnon D, Amorim J, Nahorny J, Touzeau M and Vialle M 1995 On the use of actinometry to measure the dissociation in O_2DC glow discharges: determination of the wall recombination probability *J. Phys. D: Appl. Phys.* **28** 1856–68
[5] Czerwiec T, Greer F and Graves D B 2005 Nitrogen dissociation in a low pressure cylindrical ICP discharge studied by actinometry and mass spectrometry *J. Phys. D: Appl. Phys.* **38** 4278–89
[6] Morillo-Candas A S, Drag C, Booth J-P, Dias T C, Guerra V and Guaitella O 2019 Oxygen atom kinetics in CO2 plasmas ignited in a DC glow discharge *Plasma Sources Sci. Technol.* **28** 075010
[7] Tsutsumi T, Greb A, Gibson A R, Hori M, O'Connell D and Gans T 2017 Investigation of the radially resolved oxygen dissociation degree and local mean electron energy in oxygen plasmas in contact with different surface materials *J. Appl. Phys.* **121** 143301
[8] Bernatskiy A and Ochkin V 2015 Detection of water impurities in plasma by optical actinometry *Bull. Lebedev Phys. Inst.* **42** 273–6
[9] Bernatskiy A V, Ochkin V N and Kochetov I V 2016 Multispectral actinometry of water and water-derivative molecules in moist, inert gas discharge plasmas *J. Phys. D: Appl. Phys.* **49** 395204

[10] Bernatskiy A V, Lagunov V V, Ochkin V N and Tskhai S N 2016 Study of water molecule decomposition in plasma by diode laser spectroscopy and optical actinometry methods *Laser Phys. Lett.* **13** 075702
[11] Lopaev D V, Volynets A V, Zyryanov S M, Zotovich A I and Rakhimov A T 2017 Actinometry of o, n and f atoms *J. Phys. D: Appl. Phys.* **50** 075202
[12] Kuijpers L, Baratte E, Guaitella O, Booth J-P, Guerra V, de Sanden M C V and Silva T Determination of the accuracy of actinometry and line ratio techniques in an o_2 glow discharge: Part II, electric field measurements with Ar and Xe admixtures *Plasma Sources Sci. Technol.* in review
[13] Booth J-P, Guaitella O, Zhang S, Lopaev D, Zyryanov S, Rakhimova T, Voloshin D, Chukalovsky A, Volynets A and Mankelevich Y 2023 Oxygen atom and ozone kinetics in the afterglow of a pulse-modulated dc discharge in pure O2: an experimental and modelling study of surface mechanisms and ozone vibrational kinetics *Plasma Sources Sci. Technol.* **32** 095016
[14] Booth J-P *et al* 2022 Quenching of O2(b) by O(3P) atoms. Effect of gas temperature *Plasma Sources Sci. Technol.* **31** 065012
[15] Berden G and Engeln R 2009 *Cavity Ring-Down Spectroscopy: Techniques and Applications* (Wiley)
[16] Booth J, Cunge G, Biennier L, Romanini D and Kachanov A 2000 Ultraviolet cavity ring-down spectroscopy of free radicals in etching plasmas *Chem. Phys. Lett.* **317** 631–6
[17] Stancu G D, Kaddouri F, Lacoste D A and Laux C O 2010 Atmospheric pressure plasma diagnostics by OES, CRDS and TALIF *J. Phys. D: Appl. Phys.* **43** 124002
[18] Kramida A *et al* 2021 NIST Atomic Spectra Database (ver. 5.9) (National Institute of Standards and Technology) (available at: https://physics.nist.gov/asd) (Accessed 2 October 2022)
[19] Krištof J, Annušová A, Anguš M, Veis P, Yang X, Angot T, Roubin P and Cartry G 2016 Diagnostics of low-pressure hydrogen discharge created in a 13.56 MHz RF plasma reactor *Phys. Scr.* **91** 074009
[20] Caplinger J E and Perram G P 2020 The importance of cascade emission and metastable excitation in modeling strong atomic oxygen lines in laboratory plasmas *Plasma Sources Sci. Technol.* **29** 015011
[21] Germany G A, Anderson R J and Salamo G J 1988 Electron impact excitation of the 3p(5P) state of atomic oxygen *J. Chem. Phys.* **89** 1999–2002
[22] Donkó Z, Tsankov T V, Hartmann P, Arellano F J, Czarnetzki U and Hamaguchi S 2024 Self-consistent calculation of the optical emission spectrum of an argon capacitively coupled plasma based on the coupling of particle simulation with a collisional-radiative model *J. Phys. D: Appl. Phys.* **57** 375209
[23] Julienne P S and Davis J 1976 Cascade and radiation trapping effects on atmospheric atomic oxygen emission excited by electron impact *J. Geophys. Res.* **81** 1397–403
[24] Walkup R E, Saenger K L and Selwyn G S 1986 Studies of atomic oxygen in O2+CF4 RF discharges by two-photon laser-induced fluorescence and optical emission spectroscopy *J. Chem. Phys.* **84** 2668–74
[25] Booth J P, Joubert O, Pelletier J and Sadeghi N 1991 Oxygen atom actinometry reinvestigated: comparison with absolute measurements by resonance absorption at 130 nm *J. Appl. Phys.* **69** 618–26
[26] Schulman M B, Sharpton F A, Chung S, Lin C C and Anderson L W 1985 Emission from oxygen atoms produced by electron-impact dissociative excitation of oxygen molecules *Phys. Rev. A* **32** 2100–16
[27] Niemi K, von der Gathen V S and Döbele H F 2005 Absolute atomic oxygen density measurements by two-photon absorption laser-induced fluorescence spectroscopy in an RF-excited atmospheric pressure plasma jet *Plasma Sources Sci. Technol.* **14** 375–86
[28] Xu J, Setser D and Ku J 1986 Xenon oxide and xenon sulfide emission systems at 234 and 227 nm *Chem. Phys. Lett.* **132** 427–36
[29] Laher R R and Gilmore F R 1990 Updated excitation and ionization cross sections for electron impact on atomic oxygen *J. Phys. Chem. Ref. Data* **19** 277–305
[30] Drag C, Marmuse F and Blondel C 2021 Measurement of the two-photon excitation cross-section of the 6p'[3/2]2 and 6p'[1/2]0 levels of Xe i at the wavelengths 224.3 and 222.6 nm *Plasma Sources Sci. Technol.* **30** 075026
[31] Britun N, Belosludtsev A, Silva T and Snyders R 2017 Ground state atomic oxygen in high-power impulse magnetron sputtering: a quantitative study *J. Phys. D: Appl. Phys.* **50** 075204
[32] Britun N and Hnilica J 2020 Optical spectroscopy for sputtering process characterization *J. Appl. Phys.* **127** 211101
[33] Chilton J E, Boffard J B, Schappe R S and Lin C C 1998 Measurement of electron-impact excitation into the $3p^5 4p$ levels of argon using Fourier-transform spectroscopy *Phys. Rev. A* **57** 267–77
[34] Tayal S S and Zatsarinny O 2016 *b*-spline *r*-matrix-with-pseudostates approach for excitation and ionization of atomic oxygen by electron collisions *Phys. Rev. A* **94** 042707
[35] Barklem P S 2007 Electron-impact excitation of neutral oxygen *A A* **462** 781–8
[36] Davis J, Kepple P C and Blaha M 1979 Distorted wave calculations for gaunt factors, cross sections and rate coefficients of selected al- lowed, forbidden and spin exchange transitions *Memorandum Report* (Naval Research Laboratory)
[37] Gulcicek E E and Doering J P 1987 Absolute differential and integral electron excitation cross sections of the atomic oxygen ^{3}p and 5 p states at 30 ev *J. Geophys. Res.* **92** 3445–8
[38] Gulcicek E E, Doering J P and Vaughan S O 1988 Absolute differential and integral electron excitation cross sections for atomic oxygen, 6, the 3p → 3p and 3p → 5p transitions from 13.87 to 100 ev *J. Geophys. Res.* **93** 5885–9
[39] Vaughan S O and Doering J P 1988 Absolute experimental differential and integral electron excitation cross sections for atomic oxygen: 4. the (^{3}p → 3s′^{3}p°), (^{3}p → 2s 2p 5 ^{3}p°), (^{3}p → 4d' ^{3}p°) autoionizing transitions (878, 792 and 770 Å) and five members of the (^{3}p → nd ^{3}d°) Rydberg series (1027 Å) *J. Geophys. Res.* **93** 289–93
[40] Kanik I, Johnson P V, Das M B, Khakoo M A and Tayal S S 2001 Electron-impact studies of atomic oxygen: I. differential and integral cross sections experiment and theory *J. Phys. B: At. Mol. Opt. Phys.* **34** 2647–65
[41] Viegas P, Vialetto L, van de Steeg A W, Wolf A J, Bongers W A, van Rooij G J, van de Sanden M C M, Diomede P and Peeters F J J 2021 Resolving discharge parameters from atomic oxygen emission *Plasma Sources Sci. Technol.* **30** 065022
[42] Fiebrandt M, Bibinov N and Awakowicz P 2020 Determination of atomic oxygen state densities in a double inductively coupled plasma using optical emission and absorption spectroscopy and probe measurements *Plasma Sources Sci. Technol.* **29** 045018
[43] Puech V and Torchin L 1986 Collision cross sections and electron swarm parameters in argon *J. Phys. D: Appl. Phys.* **19** 2309–23
[44] Zatsarinny O, Wang Y and Bartschat K 2014 Electron-impact excitation of argon at intermediate energies *Phys. Rev. A* **89** 022706
[45] Hayashi M 2003 Bibliography of electron and photon cross sections with atoms and molecules published in the 20th Century. Argon
[46] Bubelev V E and Grum-Grzhimailo A N 1991 Excitation of Ar I 3p54p, 3p53d and 3p55s configurations by electrons in the distorted-wave approximation *J. Phys. B: At. Mol. Opt. Phys.* **24** 2183
[47] Dasgupta A, Blaha M and Giuliani J L 1999 Electron-impact excitation from the ground and the metastable levels of Ar I *Phys. Rev. A* **61** 012703

[48] Pitchford L C et al 2013 Comparisons of sets of electron-neutral scattering cross sections and swarm parameters in noble gases: I. Argon J. Phys. D: Appl. Phys. 46 334001
[49] Chutjian A and Cartwright D C 1981 Electron-impact excitation of electronic states in argon at incident energies between 16 and 100 ev Phys. Rev. A 23 2178–93
[50] Filipovic D M, Marinkovic B P, Pejcev V and Vuskovic L 2000 Electron-impact excitation of argon: I. The 4s'$[1/2]_1$, 4p$[1/2]_1$and 4p'$[1/2]_0$states J. Phys. B: At. Mol. Opt. Phys. 33 677–91
[51] Filipovic D M, Marinkovic B P, Pejcev V and Vuskovic L 2000 Electron-impact excitation of argon: II. The lowest resonance 4s$[_3/_2]_1$and metastable 4s$[_3/_2]_2$and 4s'[Â1/2]$_0$states J. Phys. B: At. Mol. Opt. Phys. 33 2081–94
[52] Frost L S and Phelps A V 1964 Momentum-transfer cross sections for slow electrons in He, Ar, Kr and Xe from transport coefficients Phys. Rev. 136 A1538–45
[53] Bretagne J, Callede G, Legentil M and Puech V 1986 Relativistic electron-beam-produced plasmas. i. collision cross sections and loss function in argon J. Phys. D: Appl. Phys. 19 761–77
[54] Schaper M and Scheibner H 1969 Absolutbestimmung der gesamtanregungsquerschnitte der edelgase durch elektronenstoss Beitr. Plasmaphys. 9 45–57
[55] Ballou J K, Lin C C and Fajen F E 1973 Electron-impact excitation of the argon atom Phys. Rev. A 8 1797–807
[56] Albat R, Gruen N and Wirsam B 1975 Calculated born and four-state cross sections of low lying ar levels excited by proton and electron impact J. Phys. B: At. Mol. Phys. 8 L82
[57] Bogdanova I P and Yurgenson S V 1987 Cross sections for direct electronic excitation of atomic levels: measurements using a pulsed electron beam and time-base scanning of radiation. 2: Argon, $3p^5$4p level Opt. Spectros. 62 281–2
[58] Baranov V J et al Preprinf IAE-3080
[59] Priti R K G and Srivastava R 2019 Collisional-radiative model of xenon plasma with calculated electron-impact fine-structure excitation cross-sections Plasma Sources Sci. Technol. 28 025003
[60] Chiu Y-H, Austin B L, Williams S, Dressler R A and Karabadzhak G F 2006 Passive optical diagnostic of Xe-propelled Hall thrusters. I. Emission cross sections J. Appl. Phys. 99 113304
[61] Fons J T and Lin C C 1998 Measurement of the cross sections for electron-impact excitation into the $5p^5 6p$ levels of xenon Phys. Rev. A 58 4603–15
[62] Zatsarinny O and Bartschat K 2010 Benchmark calculations for near-threshold electron-impact excitation of krypton and xenon atoms J. Phys. B: At. Mol. Opt. Phys. 43 074031
[63] Buckman S J, Hammond P, King G C and Read F H 1983 High-resolution electron impact excitation functions of metastable states of neon, argon, krypton and xenon J. Phys. B: At. Mol. Phys. 16 4219–36
[64] Gousset G, Ferreira C M, Pinheiro M, Sa P A, Touzeau M, Vialle M and Loureiro J 1991 Electron and heavy-particle kinetics in the low pressure oxygen positive column J. Phys. D: Appl. Phys. 24 290–300
[65] Price D A, Lucas J and Moruzzi J L 1972 Ionization in oxygen-hydrogen mixtures J. Phys. D: Appl. Phys. 5 1249–59
[66] Price D A, Lucas J and Moruzzi J L 1973 Current growth in oxygen J. Phys. D: Appl. Phys. 6 1514–24
[67] Corbin R J and Frommhold L 1974 The first Townsend coefficient α Phys. Rev. A 10 2273–9
[68] Yanguas-Gil A, Cotrino J and Alves L L 2005 An update of argon inelastic cross sections for plasma discharges J. Phys. D: Appl. Phys. 38 1588–98
[69] Biagi S 2015 (available at: www.lxcat.net/Biagi)
[70] Meler U, Kohse-Höinghaus K and Just H 1986 H and o atom detection for combustion applications: study of quenching and laser photolysis effects Chem. Phys. Lett. 126 567–73
[71] Dagdigian P J, Forch B E and Miziolek A W 1988 Collisional transfer between and quenching of the 3p 3p and 5p states of the oxygen atom Chem. Phys. Lett. 148 299–308
[72] del Caz A T 2019 The Lisbon kinetics Boltzmann solver Plasma Sources Sci. Technol. 28 043001
[73] del Caz A T, Guerra V, Pinhão N, Pintassilgo C D and Alves L L 2021 On the quasi-stationary approach to solve the electron Boltzmann equation in pulsed plasmas Plasma Sources Sci. Technol. 30 065008
[74] Booth J-P et al 2020 Determination of absolute O(3P) and O2(a1Dg) densities and kinetics in fully modulated O2 dc glow discharges from the O2(X3Sg-) afterglow recovery dynamics Plasma Sources Sci. Technol. 29 115009